

A Survey for Redshifted Molecular and Atomic Absorption Lines

II. Associated H I, OH and millimetre lines in the $z \gtrsim 3$ Parkes Quarter-Jansky Flat-spectrum

Sample

S. J. Curran^{1*}, M. T. Whiting^{1,2}, T. Wiklind^{3,4}, J. K. Webb¹, M. T. Murphy^{5,7}, C. R. Purcell^{1,6}

¹*School of Physics, University of New South Wales, Sydney NSW 2052, Australia*

²*CSIRO Australia Telescope National Facility, PO Box 76, Epping NSW 1710, Australia*

³*Onsala Space Observatory, S-439 92 Onsala, Sweden*

⁴*Space Telescope Science Institute, Baltimore, Maryland 21218, USA*

⁵*Institute of Astronomy, Madingley Road, Cambridge CB3 0HA, UK*

⁶*Jodrell Bank Centre for Astrophysics, University of Manchester, Alan Turing Building, Oxford Road, Manchester M13 9PL, UK*

⁷*Centre for Astrophysics and Supercomputing, Swinburne University of Technology, PO Box 218, Hawthorn, VIC 3122, Australia*

Accepted —. Received —; in original form —

ABSTRACT

We present the results of a $z \gtrsim 2.9$ survey for H I 21-cm and molecular absorption in the hosts of radio quasars using the Giant Metrewave Radio Telescope and the Tidbinbilla 70-m telescope. Although the atomic gas has been searched to limits capable of detecting most known absorption systems, no H I was detected in any of the ten sources. Previously published searches, which are overwhelmingly at redshifts of $z \lesssim 1$, exhibit a 42% detection rate (31 out of 73 sources), whereas the inclusion of our survey yields a 17% detection rate (2 out of 12 sources) at $z > 2.5$. We therefore believe that our high redshift selection is responsible for our exclusive non-detections, and find that at ultra-violet luminosities of $L_{UV} \gtrsim 10^{23}$ W Hz^{−1}, 21-cm absorption has never been detected. We also find this to not only apply to our targets, but also those at low redshift exhibiting similar luminosities, giving zero detections out of a total of 16 sources over $z = 0.24$ to 3.8. This is in contrast to the $L_{UV} \lesssim 10^{23}$ W Hz^{−1} sources where there is a near 50% detection rate of 21-cm absorption.

The mix of 21-cm detections and non-detections is currently attributed to orientation effects, where according to unified schemes of active galactic nuclei, 21-cm absorption is more likely to occur in sources designated as radio galaxies (type-2 objects, where the nucleus is viewed through dense obscuring circumnuclear gas) than in quasars (type-1 objects, where we have a direct view to the nucleus). However, due to the exclusively high ultra-violet luminosities of our targets it is not clear whether orientation effects *alone* can wholly account for the distribution, although there exists the possibility that the large luminosities are indicative of a changing demographic of galaxy types. We also find that below luminosities of $L_{UV} \sim 10^{23}$ W Hz^{−1}, *both* type-1 and type-2 objects have a 50% likelihood of exhibiting 21-cm absorption.

Finally, we do not detect molecular gas in any of the sources. The lack of H I absorption, combined with the results from Paper I, suggest these sources are not conducive to high molecular abundances.

Key words: radio lines: galaxies – galaxies: active – quasars: absorption lines – cosmology: observations – galaxies: abundances – galaxies: high redshift

1 INTRODUCTION

Redshifted molecular and atomic absorption lines can provide excellent probes of the contents and nature of the early Universe. In particular, with redshifted radio and microwave lines we can

investigate the gaseous content and large-scale structure as well as any possible variations in the values of the fundamental constants at large look-back times. However, these are currently rare, with only 67 H I 21-cm absorption systems at $z \gtrsim 0.1$ known, comprising of 37 associated systems and 30 intervening (Table 1). For molecular absorption in the radio band the situation is considerably worse with only five redshifted OH 18-cm systems currently known

* E-mail: sjc@phys.unsw.edu.au

Table 1. The known redshifted ($z_{\text{abs}} \gtrsim 0.1$) H I 21-cm absorbers (updated from Paper I, Curran et al. 2006). Absorber types are: BLRG–broad line radio galaxy, CSO–compact symmetric object, CSS–compact steep spectrum source, DLA–damped Lyman- α absorption system (Mg II–DLA candidate), GPS–gigahertz peaked spectrum source, HFP – high frequency peaker galaxy, Lens–gravitational lens, OHM–OH megamaser, Red–red quasar, RG–radio galaxy. The number of each type is given, as well as the absorption redshift and column density ranges.

Reference	Type	No.	z_{abs}	$N_{\text{HI}} [\text{cm}^{-2}]$
ASSOCIATED ABSORBERS				
Mirabel (1989)	RG	2	0.10 & 0.12	$2 \text{ \& } 6 \times 10^{18} \cdot (T_s/f)$
van Gorkom et al. (1989)	RG	2	0.06 & 0.10	$11 \text{ \& } 8 \times 10^{18} \cdot (T_s/f)$
Uson et al. (1991)	RG	1	3.40	$3 \times 10^{18} \cdot (T_s/f)$
Carilli et al. (1992)	Red	1	0.25	$1 \times 10^{19} \cdot (T_s/f)$
Carilli et al. (1998)	Red	3	0.58–0.67	$0.8 - 8 \times 10^{19} \cdot (T_s/f)$
Moore et al. (1999)	Red	1	2.64	$8 \times 10^{18} \cdot (T_s/f)$
Peck et al. (1999)	CSO	1	0.10	$3 \times 10^{19} \cdot (T_s/f)$
Peck et al. (2000)	CSO	1	0.25	$5 \times 10^{18} \cdot (T_s/f)$
Ishwara-Chandra et al. (2003)	CSS/Red	1	1.19	$4 \times 10^{19} \cdot (T_s/f)$
Vermeulen et al. (2003)	BLRG	1	0.22	$7 \times 10^{17} \cdot (T_s/f)$
...	CSS	7	0.19–0.80	$0.1 - 2 \times 10^{18} \cdot (T_s/f)$
...	GPS	10	0.08–0.65	$0.07 - 3 \times 10^{19} \cdot (T_s/f)$
...	RG	1	0.24	$1 \times 10^{18} \cdot (T_s/f)$
Pihlström et al. (2005)	OHM	1	0.22	$6 \times 10^{18} \cdot (T_s/f)$
Curran et al. (2006)	RG	1	0.10	$4 \times 10^{19} \cdot (T_s/f)$
Gupta & Saikia (2006a)	RG	1	0.08	$6 \times 10^{18} \cdot (T_s/f)$
Gupta et al. (2006)	CSS	1	0.17	$5 \times 10^{18} \cdot (T_s/f)$
Orienti et al. (2006)*	HFP	1	0.67	$8 \times 10^{19} \cdot (T_s/f)$
INTERVENING ABSORBERS				
Carilli et al. (1993)	Lens	1	0.69	$1 \times 10^{19} \cdot (T_s/f)$
Lovell et al. (1996)	Lens	1	0.19	$\approx 2 \times 10^{18} \cdot (T_s/f)$
Chengalur et al. (1999)	Lens	1	0.89	$1 \times 10^{19} \cdot (T_s/f)$
Kanekar & Briggs (2003)	Lens	1	0.76	$1 \times 10^{19} \cdot (T_s/f)$
Kanekar & Chengalur (2003) [†]	DLA	15	0.09–2.04	$0.02 - 6 \times 10^{19} \cdot (T_s/f)$
Darling et al. (2004)	DLA	1	0.78	$2 \times 10^{19} \cdot (T_s/f)$
Kanekar et al. (2006)	DLA	1	2.35	$4 \times 10^{17} \cdot (T_s/f)$
Kanekar et al. (2007)	DLA	1	3.39	$1 \times 10^{18} \cdot (T_s/f)$
Gupta et al. (2007)	Mg II	3	1.17–1.37	$0.4 - 2 \times 10^{18} \cdot (T_s/f)$
Curran et al. (2007a)	Lens	1	0.96	$2 \times 10^{18} \cdot (T_s/f)$
Curran et al. (2007b)	DLA	1	0.66	$4 \times 10^{18} \cdot (T_s/f)$
York et al. (2007)	DLA	1	2.29	$2 \times 10^{18} \cdot (T_s/f)$
Zwaan et al. (in prep.)	Mg II	2	~ 0.6	–

Notes: *Also J1407+2827, which is counted as one of the 10 GPSs of Vermeulen et al. (2003).

[†]See the paper for the full reference list and Curran et al. (2005) for the calculated column densities. Note that since PKS 1413+135 is an associated system, it has been included in the top panel.

(Chengalur et al. 1999; Kanekar & Chengalur 2002; Kanekar et al. 2003), four of which also exhibit a plethora of molecular absorption lines in the millimetre regime (see Combes & Wiklind 1998).

From our previous survey for radio absorption lines in the hosts of the sources in the Parkes Half-Jansky Flat-spectrum Sample (PHFS), one H I absorption system was clearly detected (out of five searched) and one OH system tentatively detected (of the 13 searched), both at $z_{\text{abs}} \sim 0.1$ (Paper I). Upon examination of the previous detections, we concluded:

- For the H I 21-cm absorption there is no overwhelming correlation between the line strength and the optical–near-infrared ($V - K$) colour.
- However, for the OH 18-cm absorption there is a clear relationship, thus suggesting that the reddening of these quasars is due

to dust, the amount of which is correlated with the molecular abundance. Furthermore, for the molecular absorbers:

- All of the absorption lines were found at redshifts where absorption (usually H I) was already known to occur¹.
- In all cases the absorption occurs towards flat spectrum radio sources, suggesting compact radio sources and thus a large effective coverage by the absorber.

Unfortunately, prior to the analysis undertaken in Paper I, not all of the above criteria were fully formulated, and so we have also

¹ Except in the case of PKS 1830–211 where a gravitational lens of undetermined redshift was previously known (Subrahmanyan et al. 1990). The redshift was finally determined through a 14 GHz wide spectral scan of the 3-mm band (Wiklind & Combes 1996a).

targetted sources for which only the last criterion is satisfied. In this paper we present the results of a survey for redshifted atomic and molecular absorption within the hosts of sources selected from the Parkes Quarter-Jansky Flat-spectrum Sample (PQFS, Jackson et al. 2002).

Due to the search for coincident molecular absorption, we initially prioritised sources in which the $\text{HCO}^+ 0 \rightarrow 1$ transition would be redshifted into the 12-mm band of the Tidbinbilla 70-m telescope. This gave 70 targets at $z > 2.3$ out of the 878 PQFS sources, and limiting the sample further to sources with flux densities in excess of 0.5 Jy at ≈ 0.4 GHz, gave a total of 19 sources at $z > 2.9$.

2 OBSERVATIONS AND RESULTS

2.1 The redshifted decimetre wave observations

The redshifted decimetre wave observations were performed with the Giant Metrewave Radio Telescope (GMRT)² in March 2004, during the first run as described in Paper I. Again, as per Paper I, we searched for absorption within the host at the emission redshift of the quasar. Our target sample therefore consisted (primarily) of objects in the PQFS where either the H I 21-cm or OH 18-cm ($^2\Pi_{3/2} J = 3/2$) transition was redshifted into the 90-cm (≈ 327 MHz) band. Due to time constraints during the observations, we prioritised the targets in which $B \gtrsim 19$, in order to preferentially select sources where the presence of dust, associated with dense gas, would dim the visible and ultra-violet light. This left 13 out of the original 19 targets (see Table 2).

We used all 30 antennae and the 90-cm receiver over a 2 MHz bandwidth (giving a coverage of $\approx \pm 900$ km s⁻¹). Over the 128 channels (2 polarisations) this gave a channel width of 16 kHz, or a velocity resolution of ≈ 15 km s⁻¹. For all of the runs we used 3C 48, 3C 147 and 3C 286 for bandpass calibration and used separate phase calibrators for all of the sources, as heavy flagging of the target data could result in poor self calibration. The flagging and all of the reduction was done by the MIRIAD interferometry reduction package. Synthesised beam sizes were typically $\gtrsim 10''$ for the 90-cm and $\approx 6''$ for the 21-cm observations (OH $^2\Pi_{1/2} J = 1/2$ redshifted from 6-cm). As per the other observations (Paper I), channel 117 of the RR polarisation and the telescope pairing between antennae E02 and E03 (15 and 16 in AIPS/MIRIAD convention), were removed. Phase stability on all but the shortest baselines was excellent. In this band radio frequency interference (RFI) was considerably more severe than at 21-cm & 50-cm (Paper I). Regarding each source:

0335-122 was observed for 1.5 hours at a centre frequency of 319.77 MHz. While there were no overwhelmingly bad frequencies, after flagging inferior data only 135 good antenna pairs were retained.

0347-211 was observed for 1.4 hours at a centre frequency of 360.14 MHz. This band was relatively RFI free and 300 good antenna pairs were retained.

0537-286 was observed for 1.4 hours at a centre frequency of 346.10 MHz, with 210 good antenna pairs. High amplitude spikes from 345.7 to 345.9 MHz, required the removal of these frequencies.

0913+003 was observed for 1.4 hours at a centre frequency of

348.65 MHz. A spike was also dominant over 348.1 to 348.3 MHz and the full band before 18:00 UT was swamped with RFI, leaving only 40 minutes on source over a fragmented band (347.5 to 347.9 MHz). Also, since the bandpass was observed at 17:00 UT, no gain calibration is possible for this source.

1026-084 was observed for 1.9 hours at a centre frequency of 316.03 MHz and 250 good antenna pairs were retained. Again severe RFI was present over 315.3 to 315.6 MHz and frequencies above 316.7 MHz.

1228-113 was searched for H I in a 1.4 hour observation centered on 313.69 MHz. In the 210 good antenna pairs severe RFI remained from 313.0 to 313.3 MHz, leaving little remaining band below these frequencies. Since the OH $^2\Pi_{1/2} J = 1/2$ (4751 MHz) transition at the redshift of this source fell into the 20-cm band of the GMRT, this line was searched at a centre frequency of 1049 MHz for 4.4 hours. RFI was minimal and 350 good antenna pairs were retained. 1251-407 was observed for 1.4 hours at a centre frequency of 305.38 MHz. This band was fairly clean and 285 good antenna pairings were retained.

1351-018 was searched for H I in a 1.0 hour observation centered on 301.76 MHz. Although there was no overwhelmingly apparent RFI over 300.8 to 302.7 MHz, the reference antenna was affected, and so no reliable image could be produced. The optical depth is therefore derived from the averaged visibilities of the 260 good antenna pairings. OH was also searched at a frequency of 354.23 MHz for 1.4 hours. No particular frequency was especially subject to RFI, although flagging of some affected baselines was required, leaving 310 good antenna pairs.

1535+004 was searched for H I in a 1.4 hour observation centered on 315.86 MHz. Very little RFI was present giving excellent data over the 400 good antenna pairs used. Again, since the OH $^2\Pi_{1/2} J = 1/2$ (4751 MHz) transition at the redshift of this source fell into the 20-cm band of the GMRT, this transition was searched at a centre frequency of 1056 MHz for 3.1 hours. One polarisation (LL) was severely affected by RFI, and subsequently removed, while for the remaining polarisation RFI was minimal and 370 good antenna pairs were retained.

1630-004 was observed for 1.0 hour at a centre frequency of 321.07 MHz. Unfortunately RFI totally swamped this band.

1937-101 was searched for H I in a 1.4 hour observation centered on 296.72 MHz. No major RFI was present and 300 good antenna pairs were retained. OH was also searched at a frequency of 348.31 MHz for 1.8 hours. RFI was minimal and 370 good antenna pairs were retained.

2215+02 was searched for H I in a 1.4 hour observation centered on 310.67 MHz. Although no particular frequencies were affected by RFI, only 190 antenna pairs proved to be of good quality. OH was also searched at a frequency of 364.69 MHz for 3.54 hours. Due to RFI many baseline pairs had to be removed, leaving 210 pairs. Note that the bandpass calibrator, 3C 295, used for this source is unknown to MIRIAD and so this could not be used to correct the gains for 2215+02. The flux density scale for this source (Fig. 1) should therefore not be considered as absolute. Furthermore, unlike the lower frequency H I observations, the phase stability was very poor during this observation, preventing the extraction of a high quality cube.

2245-059 was observed for 1.4 hours at a centre frequency of 330.71 MHz. This band was so dominated by RFI, that no useful data could be retained.

² The GMRT is run by the National Centre for Radio Astrophysics of the Tata Institute of Fundamental Research.

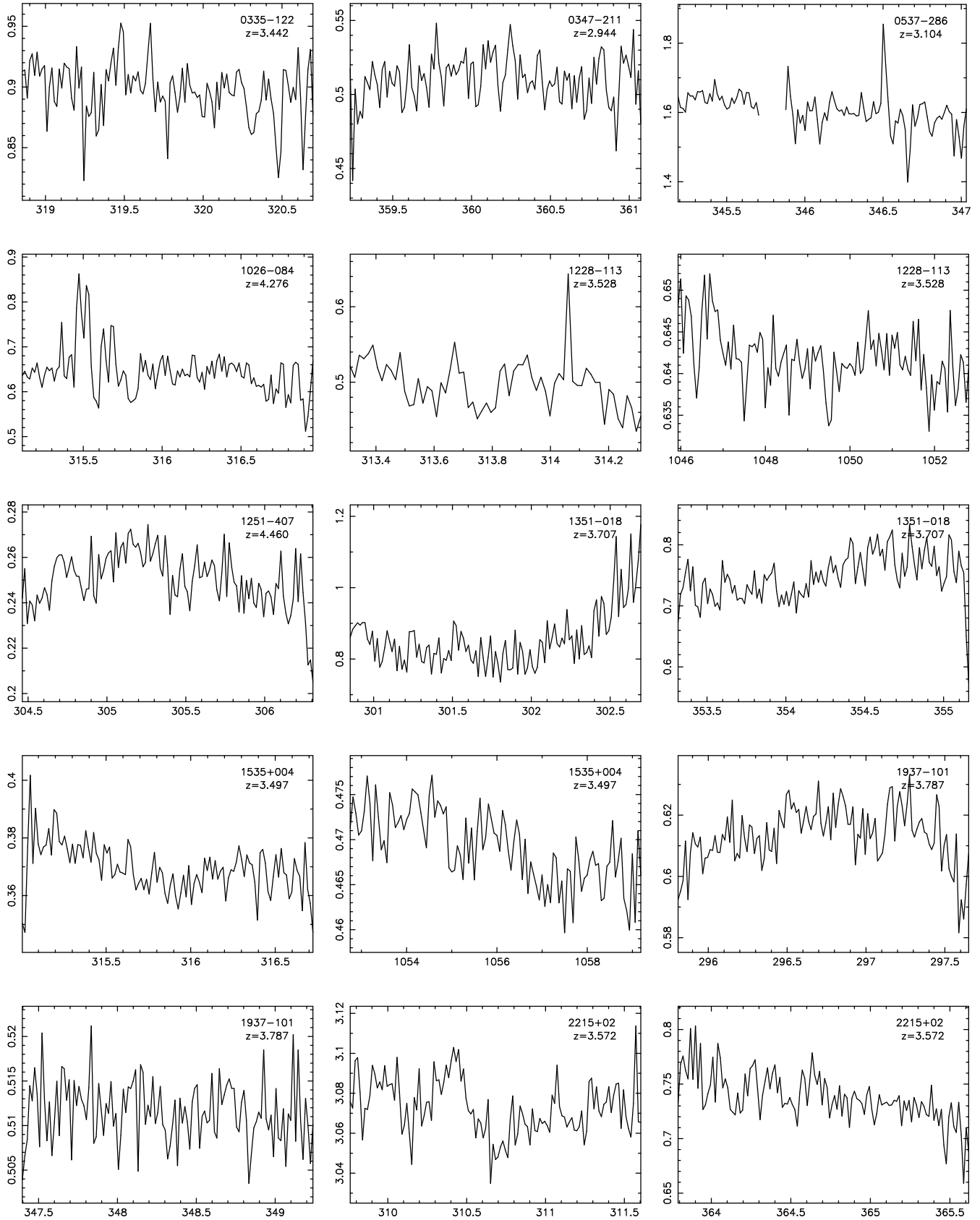


Figure 1. The GMRT spectra. The ordinate in each spectrum shows the flux density [Jy] and the abscissa the Doppler corrected frequency [MHz]. All spectra have been extracted from the spectral cube, with the exception 1351-018 at 302 MHz and 2215+02 at 365 MHz, where the visibilities are averaged together. For the latter and 2215+02 at 311 MHz the flux scale is not absolute.

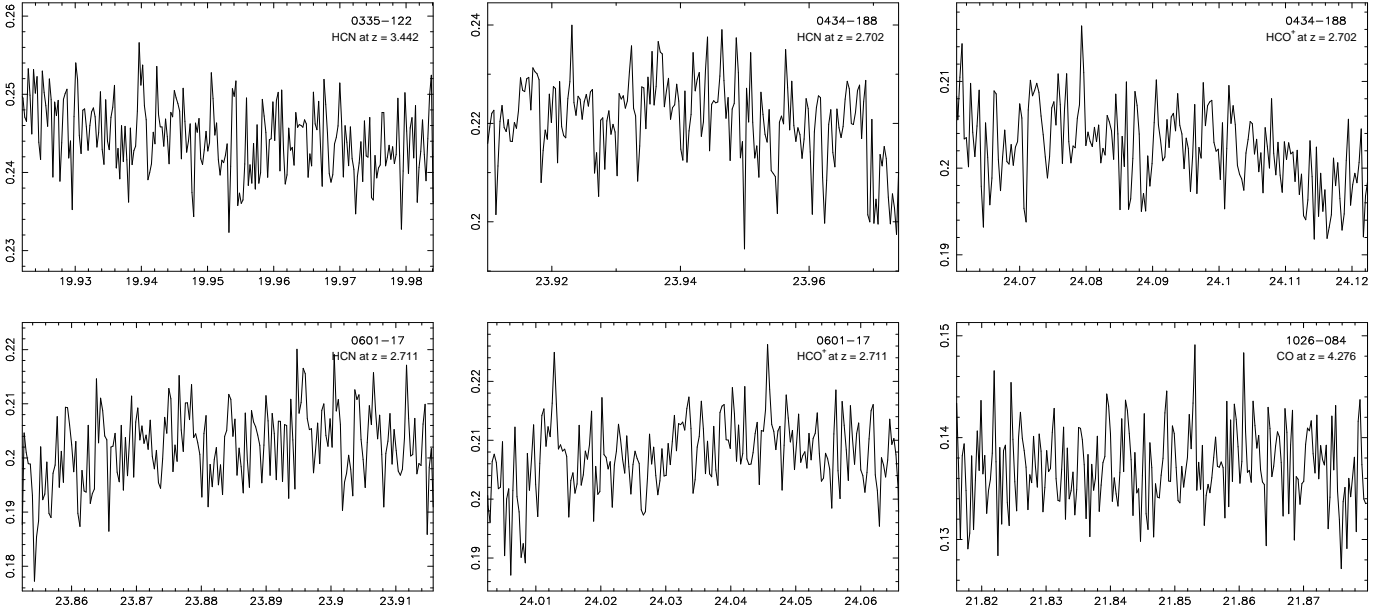


Figure 2. The Tidbinbilla spectra. The ordinate in each spectrum shows the flux density [Jy] and the abscissa the Doppler corrected frequency [GHz]. Each spectrum has been smoothed to a channel width of 4 km s^{-1} .

2.2 The redshifted millimetre wave observations

The redshifted millimetre wave observations were performed with the Australia Telescope's Tidbinbilla 70-m telescope³, over several sessions between November 2003 and March 2005. Again, the sources were selected according to those in which a strong transition⁴ fell into the 1-cm ($\approx 22 \text{ GHz}$) band. For the back-end we used the `das_xxyy_64_2048` configuration (dual polarisation with 2048 channels over a 64 MHz band), giving a resolution of $\approx 0.5 \text{ km s}^{-1}$ over a range of $\approx \pm 500 \text{ km s}^{-1}$. Such high resolution was required, since although optically thick, the line-widths in the four known millimetre absorption only span a few km s^{-1} (Wiklind & Combes 1994, 1995, 1996b, 1998), cf. up to 240 km s^{-1} for the, optically thin, OH absorption (see figure 5 of Curran et al. 2007a).

The half power beam-width (HPBW) of the single dish at these frequencies is $\approx 50''$ and, in order to ensure good baselines, we used position switching with 1 minute per position over a 4-point position switching cycle, each source being observed for a total of 4 hours. In general, the baselines were excellent with no baseline subtraction of the spectra (Fig. 2) being required. Flagging of data was only required when communication with the sub-reflector had been lost. During the observations, the T_A^* flux scale was periodically calibrated against a thermal load provided by a noise diode. An additional correction for the variation of antenna gain with elevation was applied to each spectrum off-line. The data were reduced using the DFM⁵, graphical interface to the SPC⁶ package. A quotient was formed between the source and reference

positions and the resulting spectra were averaged and weighted by $T_{\text{int}}/T_{\text{sys}}^2$. Lastly, the data were corrected onto the T_{MB} temperature scale by multiplying by the beam efficiency at 22 GHz ($\eta \approx 0.48$, Greenhill et al. 2003).

2.3 Results

In Table 2 we summarise our results. The column density is derived from the velocity integrated depth, $\tau \equiv -\ln(1 - \frac{\sigma}{fS})$, where σ is r.m.s. noise in the case of our exclusive non-detections and S and f the flux density and covering factor of the background continuum source, respectively. In the optically thin regime (where $\sigma/f.S \lesssim 0.3$), which applies to the vast majority of the known HI and all of the OH absorbers, the 1σ column density limit is given by

$$N = X \times \frac{T}{f} \int \frac{\sigma}{S} dv, \quad (1)$$

where for HI 21-cm, $X = 1.823 \times 10^{18}$ (Wolfe & Burbidge 1975) and T is the spin temperature (T_s) and for OH, $X = 2.38 \times 10^{14}$ for the $^2\Pi_{3/2}J = 3/2$ (1667 MHz) transition and $X = 1.61 \times 10^{14}$ for the $^2\Pi_{1/2}J = 1/2$ (4751 MHz) transition (Henkel et al. 1987), with T being the excitation temperature (T_x).

For OH, the values of X are derived from the total column density obtained from a rotational transition, which is given by

$$N = \frac{8\pi}{c^3} \frac{\nu^3}{g_{J+1}A_{J+1 \rightarrow J}} \frac{Qe^{E_J/kT_x}}{1 - e^{-h\nu/kT_x}} \int \tau dv, \quad (2)$$

where ν is the rest frequency of the $J \rightarrow J+1$ transition, g_{J+1} and $A_{J+1 \rightarrow J}$ are the statistical weight and the Einstein A-coefficient⁷ of the transition, respectively, and $Q = \sum_{J=0}^{\infty} g_J e^{-E_J/kT_x}$, with

⁷ These are taken from Chandra et al. (1995, 1996) or derived from the dipole moment (e.g. Rohlfs & Wilson 2000).

³ The Australia Telescope is funded by the Commonwealth of Australia for operations as a National Facility managed by CSIRO.

⁴ That is, transitions of CO, HCO⁺ and HCN, which are optically thick in the four known redshifted millimetre absorption systems.

⁵ Data From Mopra, available from <http://www.phys.unsw.edu.au/astro/mopra/software.php>

⁶ <http://www.atnf.csiro.edu.au/software>

Table 2. Summary of the search for decimetre absorption lines in the hosts of $z \gtrsim 3$ PQFS sources. ν_{obs} is the observed frequency of the line [MHz], σ_{rms} is the r.m.s. noise [mJy] reached per $\Delta\nu$ channel [km s^{-1}], S_{cont} is the continuum flux density (uncalibrated for 2215+02, Sect. 2) [Jy], τ is the optical depth of the line calculated per channel, where $\tau = 3\sigma_{\text{rms}}/S_{\text{cont}}$ is quoted for these non-detections, N is the resulting column density [cm^{-2}], where T_s is the spin temperature of the H I 21-cm line, T_x is the excitation temperature of the corresponding OH line and f the respective covering factor. In all cases OH refers to the $^2\Pi_{3/2}J = 3/2$ (1667 MHz) transition, with the exception of 1228–113 and 1534+004 for which we observed the $^2\Pi_{1/2}J = 1/2$ (4751 MHz) transition. Finally, in light of the results of Paper I, we list the V , B & K magnitudes (where available) with their respective references.

PKS	z_{em}	Line	ν_{obs}	σ_{rms}	$\Delta\nu$	S_{cont}	τ	N	z -range	B	V	K	Ref
0335–122	3.442	H I	319.77	23	15	0.90	< 0.077	$< 2.1 \times 10^{18} \cdot (T_s/f)$	3.428–3.456	21.018	20.110	17.510	1,2
0347–211	2.944	H I	360.14	17	13	0.51	< 0.10	$< 2.4 \times 10^{18} \cdot (T_s/f)$	2.935–2.953	20.476	–	17.900	2
0537–286	3.104	H I	346.10	54	14	1.61	< 0.10	$< 2.6 \times 10^{18} \cdot (T_s/f)$	3.092–3.106	19.290	–	16.770	2,3
...
0913+003	3.074	H I	348.65	–	13	–	–	RFI dominant	3.106–3.1088	20.998	20.775	–	2,4
1026–084	4.276	OH	316.03	53	15	0.65	< 0.24	$< 1.5 \times 10^{15} \cdot (T_x/f)$	4.265–4.283	21.070	–	–	2
1228–113	3.528	H I	313.69	26	15	0.49	< 0.16	$< 4.3 \times 10^{18} \cdot (T_s/f)$	3.516–3.532	22.010	–	16.370	5,3
...	...	OH	1049.17	3.7	18	0.64	< 0.017	$< 4.9 \times 10^{13} \cdot (T_x/f)$	3.513–3.543
1251–407	4.460	OH	305.38	12	15	0.25	< 0.14	$< 5.0 \times 10^{14} \cdot (T_x/f)$	4.442–4.478	–	23.7	–	6
1351–018	3.707	H I	301.76	–	16	–	< 0.090	$< 2.6 \times 10^{18} \cdot (T_s/f)$	3.693–3.722	21.030	19.696	17.070	7,4,3
...	...	OH	354.23	39	13	0.75	< 0.052	$< 1.6 \times 10^{14} \cdot (T_x/f)$	3.695–3.719
1535+004	3.497	H I	315.86	8.6	15	0.37	< 0.070	$< 1.9 \times 10^{18} \cdot (T_s/f)$	3.485–3.509	22.500	–	19.54	3
...	...	OH	1056.41	4.0	18	0.47	< 0.032	$< 9.4 \times 10^{13} \cdot (T_x/f)$	3.486–3.514
1630–004	3.424	H I	321.07	–	15	–	–	RFI dominant	–	–	21.81	–	8
1937–101	3.787	H I	296.72	9.4	16	0.61	< 0.046	$< 1.3 \times 10^{18} \cdot (T_s/f)$	3.773–3.802	18.800	–	13.816	2,9
...	...	OH	348.31	3.5	14	0.51	< 0.021	$< 7.0 \times 10^{13} \cdot (T_x/f)$	3.775–3.795
2215+02	3.572	H I	310.67	14	15	3.07	< 0.014	$< 3.7 \times 10^{17} \cdot (T_s/f)$	3.558–3.585	21.840	20.420	19.340	10
...	...	OH	364.69	22	13	–	< 0.089	$< 2.8 \times 10^{14} \cdot (T_x/f)$	3.561–3.583
2245–059	3.295	H I	330.71	–	14	–	–	RFI dominant	–	19.523	–	–	2

References: (1) Ellison et al. (2005), (2) SuperCOSMOS Sky Survey, Hambly et al. (2001), (3) P. Francis (priv.comm), (4) SDSS DR6, Adelman-McCarthy et al. (2008), (5) Chun et al. (2006), (6) Jackson et al. (2002), (7) Drinkwater et al. (1997), (8) Winn et al. (2002), (9) Smith & Heckman (1989), (10) Francis et al. (2000).

$g_J = 2J + 1$, is the partition function⁸. Since $kT_x \gg h\nu$ for $T_x \approx 10$ K and $\nu \lesssim 5$ GHz, Equ. 2 can be simplified to the above expression (Equ. 1)⁹. For the millimetre-wave column densities, based on the four known systems, the covering factor is expected to be close to unity (Wiklind & Combes 1994, 1995, 1996b, 1998) so, as in the optically thin regime, this can be written outside of the integral. However, for the same excitation temperatures the higher frequencies give $kT_x \sim E_J \sim h\nu$ and so the column density cannot be approximated via a linear dependence on the excitation temperature. We therefore adopt the canonical value of 10 K at $z = 0$ ¹⁰.

3 POSSIBLE EFFECTS IN THE NON-DETECTION OF ATOMIC ABSORPTION

From Table 2, it is seen that we do not detect 21-cm absorption in any of the ten sources for which good data were obtained. In our

earlier study of sources from the PHFS (Paper I), we detected 21-cm absorption in one out of four sources, although the only real difference between the PHFS and PQFS samples is that the PQFS has a lower flux limit (0.25 Jy, cf. 0.5 Jy)¹¹. However, due to our restriction that the sources are at redshifts where the $\text{HCO}^+ 0 \rightarrow 1$ transition is redshifted into the 12-mm band, unlike the previous search which spanned $z \approx 0.1 - 3.5$, our targets are all at $z \gtrsim 2.9$, where published searches have been very rare (Fig. 3): In the figure all of the sources in the hatched region are from our search (Table 2), in addition to the $z_{\text{em}} = 3.497$ quasar 1535+004 from Paper I. However, there is one 21-cm detection in this band ($z = 3.4$ in 0902+343, Uson et al. 1991) and so the high redshift selection on its own cannot be responsible for our non-detections, all of which have been searched to limits comparable to the detections.

Since we are searching for associated absorption, although covering factors may be an issue, these will not be subject to the same geometrical effects found for intervening systems: Specifically damped Lyman- α absorption systems (DLAs), where Curran & Webb (2006) show a strong correlation between low absorber/quasar angular diameter distance ratios and 21-cm detections, while high ratios are correlated with non-detections. This suggests that the absorbers located “closer” to us (in an angular sense) have significantly larger covering factors than those which share a similar angular diameter distance to the background quasar.

Therefore our lack of 21-cm detections must be due to another effect – either low neutral hydrogen column densities, high spin temperatures or low covering factors (see Equ. 1), although,

⁸ The energy of each level, E_J , is obtained from the JPL Spectral Line Catalog (Pickett et al. 1998). An on-line column density calculator based on Equ. 2 is available at <http://www.phys.unsw.edu.au/~sjc/column/>

⁹ Where the values for X are derived using a weighting factor of $\sum g_J/g_J = 16/5$ and $A_{J+1 \rightarrow J} = 7.71 \times 10^{-11} \text{ s}^{-1}$ (Carrington & Miller 1967) for the 1667 MHz transition. For the 4751 MHz transition, $\sum g_J/g_J = 8/3$ and $A_{J+1 \rightarrow J} = 7.7597 \times 10^{-10} \text{ s}^{-1}$ (<http://www.strw.leidenuniv.nl/~moldata/datafiles/oh@hfs.dat>).

¹⁰ Since we are analysing high redshift sources, we scale this with the temperature of the cosmic microwave background, $T_{\text{CMB}} = 2.73(1+z)$, giving $T_x = 17 - 21$ K over $z = 2.702 - 4.276$.

¹¹ Also a slightly stricter lower limit to the spectral index ($\alpha > -0.4$, cf. $\alpha > -0.5$, where $S_\nu \propto \nu^\alpha$).

Table 3. Summary of the search for millimetre absorption lines in the hosts of $z \gtrsim 3$ PQFS sources. ν_{obs} is the observed frequency of the line [GHz], σ_{rms} is the r.m.s. noise [mJy] reached per 4 km s^{-1} channel, S_{cont} is the continuum flux density [Jy] and τ is the optical depth of the line calculated per channel. The column density [cm^{-2}] of each molecule is calculated for $f = 1$ and an excitation temperature of $T_{\text{x}} = 10 \text{ K}$ at $z = 0$. The magnitudes, where available, are given in Table 2. For 0434–188, $B = 20.86$ (Ellison et al. 2005) & $K = 16.21$ (Drinkwater et al. 1997) and for 0601–17, $B = 20.445$ & $R = 20.172$ (Hambly et al. 2001).

PKS	z_{em}	Line	ν_{obs}	σ_{rms}	S_{cont}	τ	N	z -range
0335–122	3.442	HCN $0 \rightarrow 1$	19.953	4.5	0.245	< 0.055	$< 9.7 \times 10^{12}/f$	3.435–3.449
0434–188	2.702	HCN $0 \rightarrow 1$	23.942	8.7	0.220	< 0.12	$< 1.7 \times 10^{13}/f$	2.698–2.707
...	...	HCO ⁺ $0 \rightarrow 1$	24.092	4.6	0.202	< 0.068	$< 4.3 \times 10^{12}/f$	2.698–2.707
0601–17	2.711	HCN $0 \rightarrow 1$	23.884	7.0	0.202	< 0.10	$< 1.4 \times 10^{13}/f$	2.706–2.716
...	...	HCO ⁺ $0 \rightarrow 1$	24.034	6.3	0.207	< 0.091	$< 5.7 \times 10^{12}/f$	2.705–2.716
1026–084	4.276	CO $0 \rightarrow 1$	21.848	3.9	0.137	< 0.085	$< 7.8 \times 10^{15}/f$	4.268–4.284

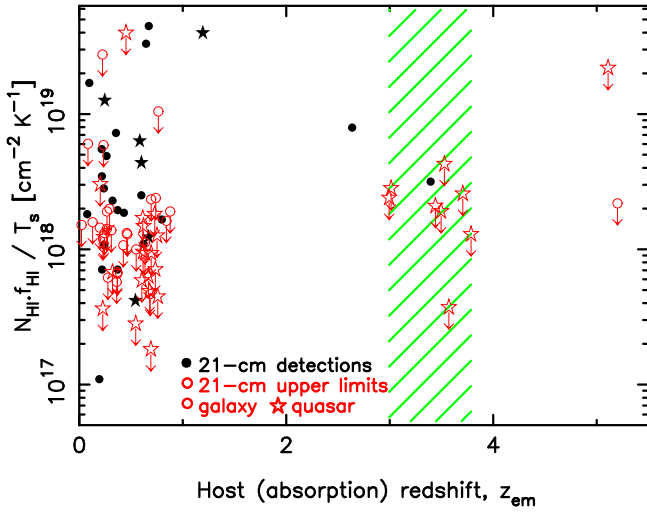


Figure 3. The scaled velocity integrated optical depth of the H I line ($1.823 \times 10^{18} \cdot \int \tau dv$) versus the host redshift for the published searches for associated 21-cm absorption (see Table 1 and Appendix A). The filled symbols represent the 21-cm detections and the unfilled symbols the non-detections, with stars designating quasars and circles galaxies (see Sect. 3.2.2). The hatched region shows the range of our H I searches (Table 2). The other results are from the references quoted in Table 1 (see Appendix A), with the addition of the two $z_{\text{em}} > 5$ non-detections of Carilli et al. (2007).

as stated, the latter would have to be due to small intrinsic absorption cross sections, since for both the 21-cm detections and non-detections in associated systems, the absorber/quasar angular diameter distance ratios are close to unity. In the absence of measurements of the neutral hydrogen column densities from the Lyman- α line, unlike DLAs, we cannot compare how N_{HI} varies between the detections and non-detections nor speculate on spin temperature effects, although Curran et al. (2005, 2007c) have shown that spin temperatures in DLAs may not vary by nearly as much as was previously believed (Kanevar & Chengalur 2003), and that these may generally be below $T_s \approx 2000 \text{ K}$ (at least up to $z_{\text{abs}} \approx 3.4$). Again, however, for these sources we have a degeneracy of three variables, all of which may be mutually coupled (see Curran et al. 2007c), thus making the relative contribution of each very difficult to ascertain.

3.1 Incident fluxes

3.1.1 21-cm luminosities

Although our sample could be highly heterogeneous, since our only criterion for our own targets is that they are high redshift PQFS sources (Sect. 1), there must be some reason why 21-cm absorption is detected in some quasars and radio galaxies, while not being detected in others, particularly at high redshift. Curran & Webb (2006) previously investigated a “proximity effect” in DLAs, where a high 21-cm flux may maintain a high population in the upper hyperfine level, thus having relatively few anti-parallel spin atoms available to absorb the 1420 MHz radiation (Wolfe & Burbidge 1975). Although there were a few non-detections and zero detections at incident flux densities of $\gtrsim 10^4 \text{ Jy}$ in this sample, there was no overwhelming trend, with the aforementioned geometrical effects being apparently much more significant with regard to the detection of 21-m absorption.

When we consider our sample, we cannot determine incident fluxes for the non-detections, as we have no knowledge of where the neutral gas would be located relative to the emission region. However, since we are just looking for statistical differences in this sample, we can still investigate this effect through the luminosities. The specific luminosity of the quasar at the rest frame emission frequency, ν_{em} , is $L_\nu = 4\pi D_{\text{QSO}}^2 S_{\text{obs}} / (z_{\text{em}} + 1)$, where D_{QSO} is the luminosity distance to the quasar¹², S_{obs} is the observed flux density¹³ and $z_{\text{em}} + 1$ corrects for the redshifting of the frequency increment. Using this expression, in Fig. 4 we show the derived quasar frame luminosities in relation to the velocity integrated optical depth of the 21-cm absorption. From this, the vertical histograms show that, on the whole, the non-detections have been searched sufficiently deeply, many to a higher sensitivity required for the detections. The horizontal histograms show considerable overlap, and, while the average $\log L_{\text{radio}}$ is higher for the non-detections, the difference is small ($\log L_{\text{radio}} = 27.06$ cf. 26.71), and the distributions of luminosities for detections and non-detections are not statistically different (the probability of the null hypothesis for the Kolmogorov-Smirnov test is 33.7%). Therefore, although a high incident 21-cm flux may make a detection less likely through a highly populated upper hyperfine level, this does not appear to be an overwhelming cause of the non-detections.

¹² Throughout this paper we use $H_0 = 75 \text{ km s}^{-1} \text{ Mpc}^{-1}$, $\Omega_{\text{matter}} = 0.27$ and $\Omega_\Lambda = 0.73$.

¹³ Since we are searching for absorption at the host redshift, the quasar frame 21-cm flux density is given by the observed value.

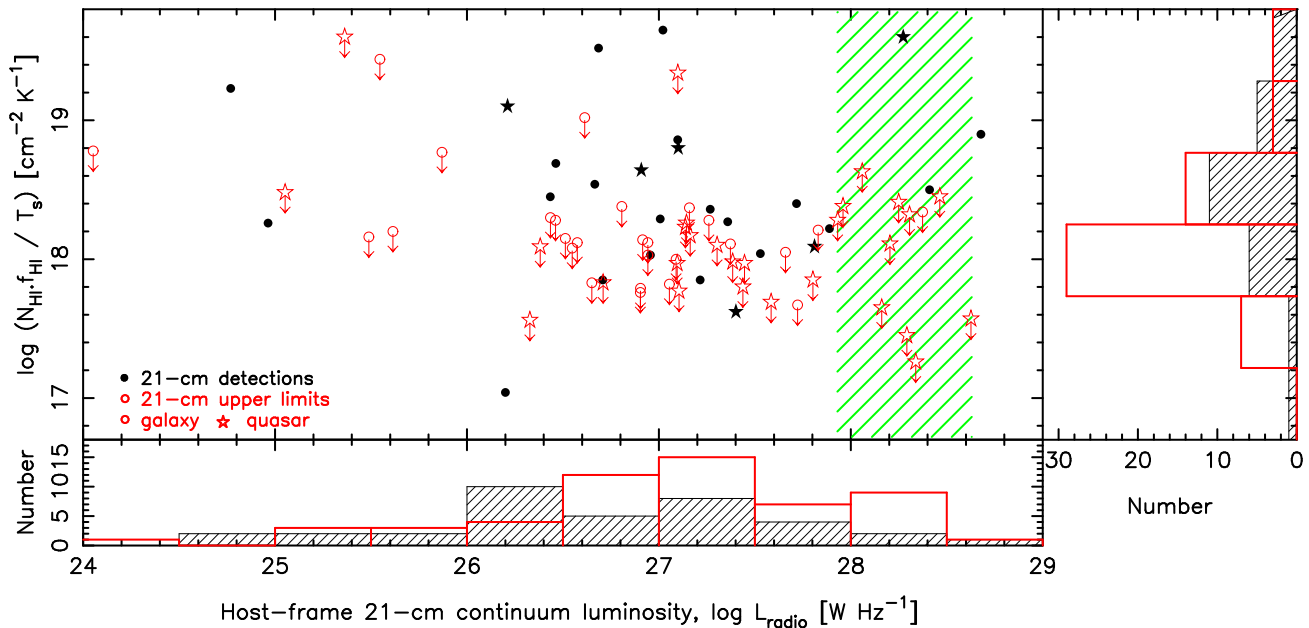


Figure 4. The scaled velocity integrated optical depth of the H I line versus the quasar frame 21-cm luminosity for the quasars searched for associated H I absorption. Again, the hatched region shows the range of our H I searches. Throughout this paper the filled symbols/hatched histogram represent the 21-cm detections and the unfilled symbols/coloured histogram the non-detections.

3.1.2 Ultra-violet luminosities

Although a 21-cm proximity effect is not apparent for DLAs or associated absorbers, in the ultra-violet such an effect is well known, where a high ionising flux from the quasar is believed to be responsible for the decrease in the number density of the ultra-violet Lyman- α lines as z_{abs} approaches z_{em} (Weymann et al. 1981; Bajtlik et al. 1988). To excite the hydrogen beyond the realm of 21-cm absorption does not require ionisation of the gas (by 912 Å photons), but “merely” excitation above the ground state by a Lyman- α (1216 Å) photon, although the lifetime in this state is only $\sim 10^{-8}$ s. In any case, since both the ionising and Lyman- α photons are $\sim 10^6$ times as energetic as the spin-flip transition, if the gas is excited by Lyman- α absorption, much of it will also be ionised.

Therefore, in order to determine the ~ 1000 Å fluxes, we have exhaustively searched the literature and on-line archives to obtain optical and near-infrared photometry of as much of the sample as possible (see Appendix A). In some cases, we use the photometry of the Sloan Digital Sky Survey (SDSS, York et al. 2000)¹⁴, taken from Data Release 6 (Adelman-McCarthy et al. 2008), ap-

plying the transformations of Fukugita et al. (1996) to ensure consistency between the bands. From these measurements, we estimate the $\lambda \approx 1216(1+z)$ Å flux according to the prescription in Appendix B, and thence the luminosity in the rest-frame of the galaxy/quasar.

Since the sources cover a range of redshifts, the interpolations/extrapolations necessary to estimate L_{UV} involve different bands for different sources. We can check the validity of the estimates by comparing the interpolated value of the flux at the nominal 1216 Å wavelength (from *BVR*) with that extrapolated from the *JHK* bands. The latter situation is similar to the case of extrapolating from optical bands for low-redshift sources. In our sample, there are only three sources in the high ($z > 2.5$) redshift group for which we have more than one near-infrared band available: J0414+0534, 1937–101 (both of which have 2MASS¹⁵ photometry) and 2215+020 (Francis et al. 2000) and for these, we can compare the extrapolation of the *JH* measurements to that obtained from *BR*. 2215+020 has the same extrapolation for both, 1937–101 has *JH* overestimating the flux by a factor of ~ 5 , and J0414+0534 overestimates by ~ 50 . The analysis of the latter source could be affected by the extreme optical–near-IR colour of $V - K = 10.26$ (Lawrence et al. 1995) [see Sect. 4], most likely due to the presence of dust in the intervening gravitational lens or host galaxy¹⁶. The other two sources, however, show that the extrapolation from longer wavelengths (rest-frame optical) can give a value of the UV flux in broad agreement with the extrapola-

¹⁴ The SDSS is managed by the Astrophysical Research Consortium (ARC) for the Participating Institutions. The Participating Institutions are the American Museum of Natural History, Astrophysical Institute Potsdam, University of Basel, University of Cambridge, Case Western Reserve University, The University of Chicago, Drexel University, Fermilab, the Institute for Advanced Study, the Japan Participation Group, The Johns Hopkins University, the Joint Institute for Nuclear Astrophysics, the Kavli Institute for Particle Astrophysics and Cosmology, the Korean Scientist Group, the Chinese Academy of Sciences (LAMOST), Los Alamos National Laboratory, the Max-Planck-Institute for Astronomy (MPIA), the Max-Planck-Institute for Astrophysics (MPA), New Mexico State University, Ohio State University, University of Pittsburgh, University of Portsmouth, Princeton University, the United States Naval Observatory, and the University of Washington.

¹⁵ The Two Micron All Sky Survey, is a joint project of the University of Massachusetts and the Infrared Processing and Analysis Center/California Institute of Technology, funded by the National Aeronautics and Space Administration and the National Science Foundation.

¹⁶ Note that on the basis of their detection of H I in the lens in conjunction with a strong limit on the OH column density, Curran et al. (2007a) [and references therein] suggest that the reddening is occurring in the $z = 2.64$ host galaxy.

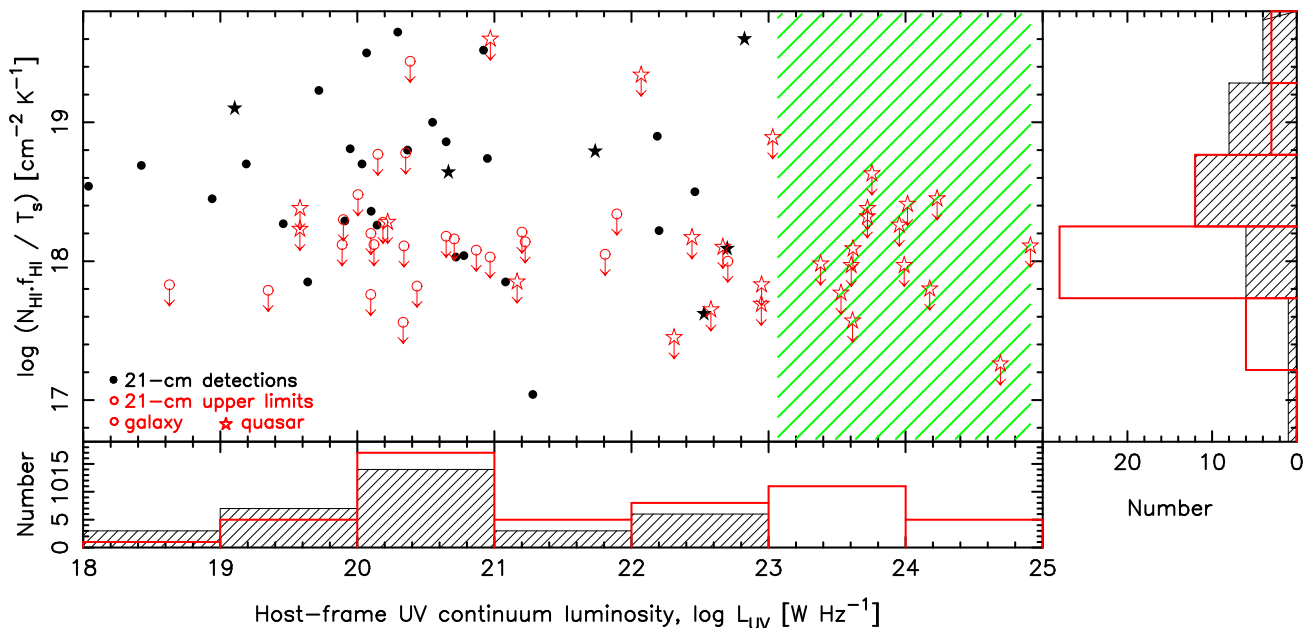


Figure 5. As per Fig. 4, but with the scaled velocity integrated optical depth of the H I line versus the quasar frame ultra-violet luminosity.

tion from rest-frame UV. We note that an extrapolation using JH for these sources is roughly equivalent to using BR for sources at $0.6 \lesssim z \lesssim 1.0$.

Plotting our results, in Fig. 5 we see an equal mix of 21-cm detections and non-detections below the median value of the UV luminosity range ($\frac{18.04+24.91}{2} = 21.48$). However, at higher luminosities the distribution is dominated by non-detections which become exclusive at $L_{UV} \gtrsim 10^{23} \text{ W Hz}^{-1}$, the range occupied by our observed sample (Table 2)¹⁷. Investigating the likelihood of such a distribution occurring by chance, defining a partition at the median of the sample gives 52 objects (26 detections & 26 non-detections) in the low luminosity bin and 33 objects (7 detections & 26 non-detections) in the $\log L_{UV} > 21.48$ bin. For an unbiased sample, i.e. there is an equal likelihood of either a detection or non-detection (as may be expected from orientation effects, see next section), the binomial probability of 26 or more detections out of 52 objects occurring is 55%. However, the probability of 25 non-detections or more out of 33 objects in the other bin is just 0.23%. Moving the partition to $\log L_{UV} = 23.0$, thus covering the range of our targets (Fig. 5), in the low luminosity bin there are 33 detections out of 69 objects (again a near 50% detection rate) and in the high luminosity bin, 0 detections out of 16. Again, assuming an unbiased sample, the binomial probability of this latter distribution is 0.0015%, a significance of 4.3σ assuming Gaussian statistics¹⁸, against the probability of a 21-cm absorption detection being unrelated to the ultra-violet luminosity. Applying a Kolmogorov-Smirnov test, there is a 99.25% confidence that the UV luminosity distribution of the detections differs from that of the non-detections. Therefore there is a relationship between the ultra-violet luminosity and the likelihood of detecting 21-cm absorption.

¹⁷ The mean luminosity of the detections is $\log L_{UV} = 20.5 \pm 1.2$, cf. $\log L_{UV} = 21.8 \pm 1.7$ for all of the non-detections and $\log L_{UV} = 20.8 \pm 1.1$ for the low luminosity non-detections.

¹⁸ Should there be an overwhelming error in the band extrapolations, to the point where the $z > 1$ luminosities cannot be used in the comparison, for the $z < 1$ sources alone the result remains significant at 2.9σ .

3.2 Orientation effects

3.2.1 Unified schemes of AGN

Previously, the mix of 21-cm detections and non-detections has been attributed to unified models of active galactic nuclei (AGN). This is an orientation effect due to the presence of a dense sub-pc circumnuclear disk or TORUS¹⁹ of gas which obscures the UV/optical light from the AGN: In type-1 objects, the obscuration has its rotation axis directed towards us and the AGN and the centralised broad-line region are viewed directly, whereas in type-2 objects the AGN is hidden, and only the more extended narrow-line region is visible (see Antonucci 1993; Urry & Padovani 1995). It is hypothesised that the 21-cm absorption occurs in this obscuration and so is only visible in type-2 objects, where the gas intercepts the line-of-sight to the AGN (e.g. Jaffe & McNamara 1994; Conway & Blanco 1995).

For instance, of four 21-cm detections in a sample of 23 $z_{\text{em}} < 0.7$ radio galaxies (Morganti et al. 2001), two are narrow-line radio galaxies, indicating type-2 objects, and the other two are weak-line radio galaxies. Therefore, superficially at least, this is consistent with the 21-cm absorption occurring in an intervening torus or disk (Morganti et al. 2001). However, the fact that there are significant redshift (velocity) offsets between the 21-cm and optical lines, leads the authors to conclude that some of the H I responsible for the absorption is located farther out than the central sub-pc occupied by the dense obscuration. The presence of significant gas motions, due to infall, outflows, jet interactions as well as general galactic rotation²⁰ is also suggested by the large velocity offsets found in a sample of 19 detections by Vermeulen et al. (2003) [see Fig. 6].

Furthermore, Pihlström et al. (2003) note that 21-cm absorption is more likely to be detected in radio galaxies than in quasars,

¹⁹ e.g. Thick Obscuration Required by Unified Schemes (Conway 1999).

²⁰ Although gas in the galactic disk may be expected to share the same orientation as the sub-pc obscuration (Curran et al. 1998, cf. Greenhill et al. 2003, see also Curran 2000a).

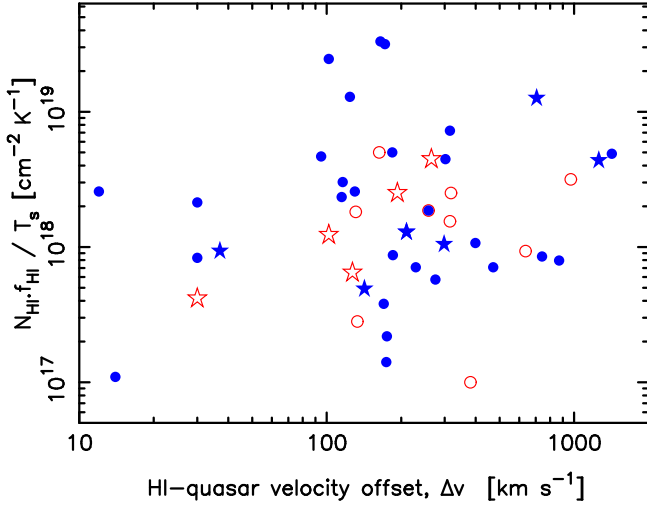


Figure 6. The 21-cm absorption strength versus the velocity offset of the 21-cm absorption from the host. Here we have plotted each individually resolved absorption component at its line strength and velocity offset for each of the detections (Table 1). The solid symbols represent blueshifted (approaching) H I and the hollow symbols redshifted (receding) H I. In associated systems these offsets represent peculiar motions rather than the Hubble flow. Furthermore, there are often velocity differences between different optical lines and so these velocities cannot be reliably converted to distance offsets to yield the incident flux on the absorbing gas.

suggesting that the quasars are viewed at lower inclinations, thus having the observed radio emission bypass the absorbing gas which obscures the optical/UV light. The orientations for a very limited sample (Pihlström et al. 2003) are quantified by the core prominence, where the galaxies have core emission fractions of $f_c < 0.03$, cf. $f_c > 0.04$ for the quasars, the larger core prominence being attributed to a more direct viewing angle to the AGN. From a larger sample, Gupta & Saikia (2006b) find that the galaxies have a median value of $f_c = 0.011$, compared to $f_c = 0.028$ for the quasars. However, the distribution becomes more mixed with nearly half of the quasars located below the median value for the galaxies ($f_c \sim 0.01$) and with five galaxies at $f_c \gtrsim 0.03$. Additionally, although none of the quasars have been detected in 21-cm absorption, all of these five galaxies exhibit strong ($N_{\text{HI}} \geq 1.6 \times 10^{18} \cdot T_s / f \text{ cm}^{-2}$) absorption, thus weakening the argument that core dominance indicates lower inclinations, or at least, the amount of cold neutral gas lying along the sight-line to the AGN.

Many of these core fractions have however been estimated²¹, and overestimates could explain the five 21-cm absorbing galaxies exhibiting a large core prominence. Nevertheless, from their CSS and GPS sample (Gupta & Saikia 2006b) there is a 21-cm detection rate of 1 out of 9 for quasars, cf. 15 out of 23 for galaxies, supporting the existence of a bias. Quantifying this, the binomial probability of 15 or more out of 23 detections occurring in one class, while 8 or more non-detections occur in another class is 0.20%, again consistent with quasars being the result of lower inclined obscuring tori.

²¹ Using assumed spectral indices and at a frequency of 8 GHz, which is an order of magnitude higher than the typical observed redshifted 21-cm frequency.

3.2.2 Quasar–galaxy classifications

The classification schemes used by these authors do not apply to all the sources under consideration in this work. We have therefore applied our own scheme in order to examine the effect of the relative strength of the quasar/AGN nucleus over the host galaxy. The aim is to distinguish sources whose appearance is dominated by the nuclear source (the “quasars”) from those whose appearance is dominated by the extended stellar light of the host galaxy (the “galaxies”). The latter sources are those with either intrinsically weaker AGN or the type-2 AGN that are obscured from the line-of-sight. The classification was mostly done on a morphological basis, using SuperCOSMOS Sky Survey images and classification (which does a star/galaxy classification based on the source profile), DSS2 images, as well as detailed imaging and spectroscopic analysis (where the spectra are examined for evidence of galaxy light or quasar emission lines) available from the literature. Each source was examined individually to ensure the classifications were consistent. There are some obvious caveats with this process. By looking at the morphology, we are biasing ourselves somewhat against high-redshift galaxies, since we lose the resolution and surface-brightness sensitivity for detecting the galaxy light. However, many of the high-redshift sources have higher-resolution imaging or spectroscopic observations available that allow us to determine the importance of the host galaxy in the source’s appearance.

In order to compare the proportions of detections and non-detections for galaxies and quasars, we use the following statistic. If we have two measured proportions $\hat{p}_1 = X_1/N_1$ and $\hat{p}_2 = X_2/N_2$, with the total proportion $\hat{p} = (X_1 + X_2)/(N_1 + N_2)$, then

$$T = \frac{\hat{p}_1 - \hat{p}_2}{[\hat{p}(1 - \hat{p})(N_1^{-1} + N_2^{-1})]^{1/2}}, \quad (3)$$

which has a standard normal distribution (mean zero, variance one) under the null hypothesis, being that the two proportions (\hat{p}_1 and \hat{p}_2) are the same. We examined the proportion of sources that we classified as galaxies (as opposed to quasars), and found that sources with detected absorption had a much higher galaxy proportion (28 out of 34) than sources without absorption (28 out of 56). These fractions are different at 99.67% confidence. Additionally, almost all the high- L_{UV} sources are “quasars” – only 1 out of the 24 sources with $L_{\text{UV}} > 10^{22.5} \text{ W Hz}^{-1}$ is a galaxy.

3.2.3 Our results in the context of the unified schemes

All of the above discussion on orientation effects applies to the low redshift sample, where searches have previously been concentrated (Fig. 3)²². Of our own low redshift searches (Paper I), one target out of three was detected in 21-cm absorption, i.e. as per the 33% detection rate of Vermeulen et al. (2003), the rate expected from unified schemes²³. For the two undetected, 1450–338 ($z = 0.368$) has an estimated UV luminosity of $L_{\text{UV}} = 4 \times 10^{18} \text{ W Hz}^{-1}$ and 2300–189 ($z = 0.129$) $L_{\text{UV}} = 1 \times 10^{20} \text{ W Hz}^{-1}$, cf. $L_{\text{UV}} = 5 \times 10^{19} \text{ W Hz}^{-1}$ for the detection in 1555–140

²² The large gap in redshift space between these and the high redshift targets (Fig. 3) is due to a lack of (RFI free) coverage over ≈ 350 to 700 MHz.

²³ The detection rate for a given half-opening angle, α , is $1 - \cos \alpha$, giving a detection rate of 29% for a randomly oriented population with a 90° opening angle.

($z = 0.097$). That is, the UV luminosity of the detection lies between those of the non-detections, although all lie well within the $L_{UV} \lesssim 10^{23} \text{ W Hz}^{-1}$ detection range (Fig. 5). Regarding their orientations, 1450–338 is an apparently dust-reddened quasar (Francis et al. 2000), 2300–189 is a Seyfert 1 galaxy, whereas the strong ($N_{\text{HI}} = 4.2 \times 10^{19} \text{ cm}^{-2}$, $T_s/f \text{ cm}^{-2}$) 21-cm absorber 1555–140 has a reddened type-2 AGN spectrum superimposed on a galaxy (Wilkes et al. 1983), and is itself a large galaxy in the centre of a group. With the one detection occurring in the only type-2 object, our low luminosity results are consistent with unified schemes, as discussed above.

However, although our high redshift criterion selects highly luminous sources, note that half (8 out of 16) of those with $L_{UV} \gtrsim 10^{23} \text{ W Hz}^{-1}$ have redshifts of $z_{\text{em}} \leq 0.73^{24}$ and, in common with the other $L_{UV} \gtrsim 10^{23} \text{ W Hz}^{-1}$ targets, these are all non-detections. This raises the question of whether orientation effects alone can account for the observed differences. That is, why do some of the low redshift non-detections exhibit low UV luminosities when, like their high luminosity counterparts, we expect to have a direct view to the UV emitting region in these type-1 objects?

3.3 The significance of known intervening absorbers

Most of our targets also have intervening DLAs and so if the photons emitted from the quasar are ionising, a significant number of these must have been redshifted to 1216 Å by time they encounter the absorber, providing a continuum for the Lyman-α absorption. In fact, DLAs could be common to many of the objects searched for host absorption, although ground based observations of the Lyman-α line are usually restricted to redshifts of $z \geq 1.7$, where the line is redshifted into optical bands²⁵. From Fig. 3, we see that only our targets, the two high- z 21-cm detections (Uson et al. 1991; Moore et al. 1999, Table 1) and the two targets of Carilli et al. (2007) are of sufficiently high redshift to illuminate such absorbers. The DLAs which intervene our targets (nine in total towards seven sources) are all themselves at redshifts ($z_{\text{abs}} \geq 1.947$), comparable to those of the background quasars (Table 4).

The redshift of the background source in the rest frame of the absorber is given by $\Delta z = \frac{z_{\text{em}}+1}{z_{\text{abs}}+1} - 1$ and at $\Delta z = 0.33$, the 912 Å (ionising) photon is redshifted to 1216 Å. All but two of the DLAs have $\Delta z < 0.33$ (Table 4), meaning that the radiation which is Lyman-α absorbed must have been non-ionising at the source. Two of the DLAs have also been searched, and not detected, in 21-cm absorption; 0335–122 and 0537–286 (Kanekar & Chengalur 2003). The non-detections place spin temperate/covering factor ratios of $T_s/f \gtrsim 2000$ and $\gtrsim 700 \text{ K}$, respectively, and since both occult very compact radio sources (Table 2 of Curran et al. 2005), f may be close to unity, indicating high spin temperatures in these absorbers (cf. Curran & Webb 2006). Therefore, as shown by these two cases, the non-detection of 21-cm does not necessarily imply a lack of neutral gas close to the quasar.

In the absence of total neutral hydrogen column densities, we cannot estimate the limits for our targets (Table 2), although for

Table 4. The targets with detected intervening DLAs ($N_{\text{HI}} \geq 2 \times 10^{20} \text{ cm}^{-2}$) and sub-DLAs. Note that 0913+003, 1026–084 & 1251–407 have not featured in any of our prior statistics since the H I search in 0913+003 was ruined by RFI and in the latter two we searched for OH only (H I is redshifted out of the band).

QSO	z_{abs}	$\log N_{\text{HI}}$	Ref.	z_{em}	Δz
0335–122	3.178	20.8	E01	3.442	0.063
0347–211	1.947	20.3	E01	2.944	0.338
0537–286	2.974	20.3	E01	3.104	0.033
0913+003	2.774	20.3	E01	3.074	0.079
1026–084	3.42	20.1	P01	4.276	0.193
...	4.05	19.7	P01	...	0.045
1228–113	2.193	20.6	E01	3.528	0.418
1251–407	3.533	20.6	E01	4.464	0.205
..	3.752	20.3	E01	...	0.150

References: E01: Ellison et al. (2001), P01: Péroux et al. (2001). Notes: No DLAs have been found towards 1351–018, 1535+004, 1937–101, 2215+02, 2245–059 (Ellison et al. 2001), 1937–101 (Lanzetta et al. 1991).

$N_{\text{HI}} \gtrsim 10^{20} \text{ cm}^{-2}$, $T_s \gtrsim 10^3 \text{ K}$, which is around the typical upper limit for the detection of 21-cm absorption in DLAs (figure 5 of Curran et al. 2007c). The spin temperature measures the relative populations of the two possible spin states (Purcell & Field 1956), although excitation to the $n = 2$ level by Lyman-α photons will also raise the spin temperature (Field 1959). Furthermore, Bahcall & Ekers (1969) show that both the 21-cm (cf. Fig. 4) and the Lyman-α (cf. Fig. 5) flux can contribute to the spin temperature at absorber–quasar separations of less than a few tens of kpc, i.e. for associated systems.

In addition to many of the background quasars of our sample emitting a large fraction of non-ionising, high energy ($1216 < \lambda < 912 \text{ Å}$) photons, there exists a number of proximate damped Lyman-α absorption systems (PDLAs), where at $\Delta v \leq 3000 \text{ km s}^{-1}$, the ionisation of the gas is expected to be dominated by the quasar, rather than the background UV flux²⁶. Unlike the detections in the associated sample (Table 1), many of the PDLAs are subject to $L_{UV} \gtrsim 10^{23} \text{ W Hz}^{-1}$ (Fig. 7). From the figure we see that few of the PDLAs appear to arise in the host (i.e. at $\Delta v \lesssim 300 \text{ km s}^{-1}$). Comparing these with the associated sample (Fig. 6), a Kolmogorov-Smirnov test on the velocity offsets gives a probability of only 9.7×10^{-12} that the associated detections and the PDLAs are drawn from the same sample. Therefore, although there are several PDLAs for which $L_{UV} \gtrsim 10^{23} \text{ W Hz}^{-1}$ at $\Delta v \lesssim 300 \text{ km s}^{-1}$, PDLAs are not (generally, at least) associated systems (see also Møller et al. 1998). That is, although it is feasible that a search for associated absorbers could overlap significantly with a search for PDLAs, we show that this is generally not the case. For the PDLAs, $\Delta z \lesssim 0.01$ and, as per the DLAs detected towards our targets (Table 4), this would suggest again that much of the flux from the quasar is non-ionising at the source²⁷.

Since, by definition, the DLAs towards our targets are subject to a high 1216 Å flux, there must be a significant portion

²⁴ This demonstrates that the segregation of our high luminosity sample is not due to a systematic underestimate in the low redshift UV luminosities, where the extrapolation of the SEDs are generally more extreme than for the high redshift sources (Sect. 3.1.2).

²⁵ Additionally, at redshifts of $z \gtrsim 4$, the increasing line density per unit redshift of the Lyman-α forest, makes the identification of DLAs very difficult.

²⁶ At $10^4 \gtrsim \Delta v \gtrsim 10^5 \text{ km s}^{-1}$ (Table 4), none of the DLAs intervening our targets are proximate.

²⁷ Since DLAs do not generally occult quasars of sufficient radio flux to be detected in 21-cm absorption at present ($\gtrsim 0.1 \text{ Jy}$, see Curran et al. 2002), it is likely to remain unknown for some time whether these PDLAs are host to cold neutral gas.

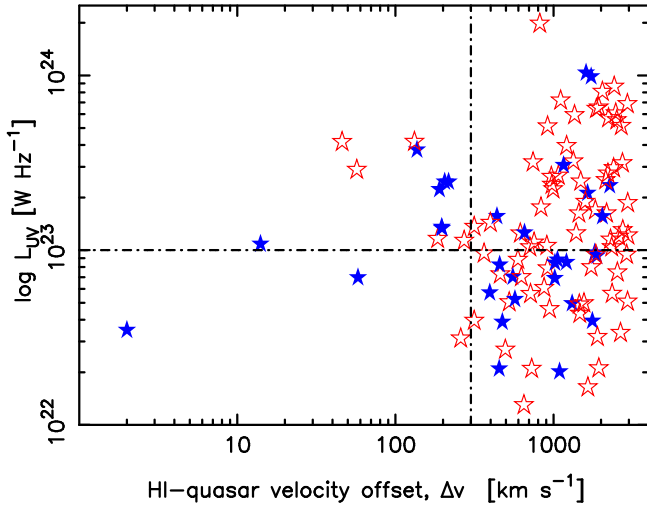


Figure 7. The ultra-violet ($\approx 912 \text{ \AA}$) luminosity versus the velocity offset of the Lyman- α absorption from the background quasar for the SDSS DR5 PDLA sample (Prochaska et al. 2008). The quasar redshifts range from $z_{\text{em}} = 2.308$ to 5.185 and the luminosities have been estimated as per the associated sample (Sect. 3.1.2). The solid symbols represent blueshifted (approaching) H I and the hollow symbols redshifted (receding) H I. The horizontal lines signifies the detection cut-off for the associated systems and the vertical line, the fiducial 300 km s^{-1} offset above which the gas is believed to be unassociated.

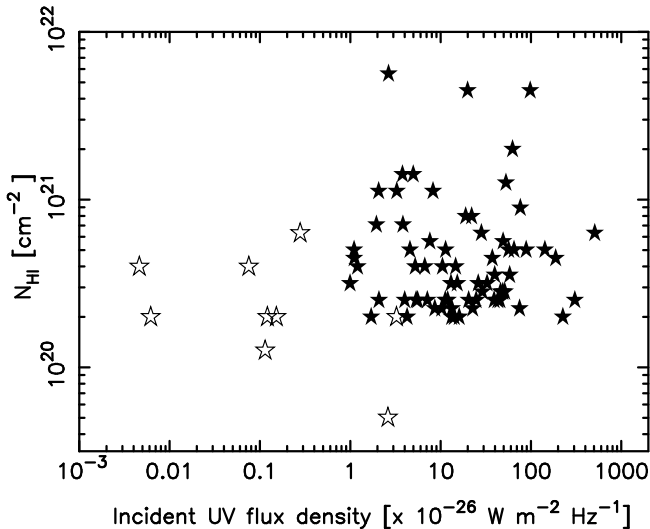


Figure 8. The neutral hydrogen column density versus the incident UV flux at the DLAs towards our targets (Table 4, unfilled markers) and the $\Delta v \geq 300 \text{ km s}^{-1}$, $z_{\text{abs}} < z_{\text{em}}$ PDLAs (Prochaska et al. 2008, filled markers). These criteria have been applied in order to select absorbers directly along the line-of-sight and with the redshifts not dominated by peculiar motions. The scatter in the distribution remains if the whole PDLA sample is used.

of ionising photons present, which could render the gas less detectable in Lyman- α (and 21-cm) absorption, although at these high column densities self-shielding effects (Zheng & Miralda-Escudé 2002) should counteract this somewhat. Note, however, that none of the sight-lines towards our targets exhibit further DLAs between those listed in Table 4 and z_{em} , where the ionising photons will be less redshifted. In Fig. 8 we convert the luminosities to fluxes for the DLAs towards our targets and the PDLA sample. Although, there is a tentative trend for the column density of the neutral gas

to decrease with flux for our targets, this is not borne out by the larger PDLA sample. Although this would suffer a selection effect by being limited to the $N_{\text{HI}} \geq 2 \times 10^{20} \text{ cm}^{-2}$ DLA defined cut-off (where self-shielding becomes particularly significant, Zheng & Miralda-Escudé 2002), at higher incident fluxes there appears to be no additional appreciable photo-ionisation. However, PDLAs are considerably less numerous than expected, which Prochaska et al. (2008) attribute to photo-evaporation. Another factor which could cover any neutral gas column density–incident UV flux anti-correlation is the possibility that the observed redshift differences between the absorbers and quasars do not provide accurate distances in these cluster environments. This could be the case for the $\Delta v \leq 300 \text{ km s}^{-1}$ PDLAs of Fig. 7.

3.4 The chicken or the egg: ionising UV flux or orientation effects

3.4.1 Orientation: Ionisation

Since Lyman- α absorption is not detected in the hosts of any of our high redshift quasar sample (Ellison et al. 2001; Péroux et al. 2001), it is not surprising that 21-cm absorption remains undetected. Naturally, intervening DLAs require sufficient background UV flux against which to detect absorption, and by selecting such high redshift sources, we are selecting those which are sufficiently luminous in the UV to enable the detection of intervening absorption, but perhaps too bright to host a large column of neutral gas close to the host.

This raises the question of whether it is the UV luminosity ionising the neutral gas, which would otherwise be there, or the distribution of the gas (a face-on torus), which is responsible for the non-detection of 21-cm absorption in these sources. For the PDLAs there are several cases where $L_{\text{UV}} \gtrsim 10^{23} \text{ W Hz}^{-1}$ in what could be associated absorption ($\Delta v \leq 300 \text{ km s}^{-1}$) and orientation effects could be consistent with the complete lack of any PDLAs in our own (admittedly, small) target sample (Table 4). This paucity may however be expected without invoking orientation effects, since PDLAs constitute only a small fraction ($\sim 5\%$) of the DLA sample (Ellison et al. 2002; Prochaska et al. 2008) and those which may be associated ($\Delta v \leq 300 \text{ km s}^{-1}$) are even rarer ($\lesssim 1\%$).

In AGN, large-scale (kpc) outflows of ionised gas, directed along the radio jets are rife (particularly in Seyfert galaxies, see table 1.2 of Curran 2000b²⁸). These are believed to be due to either nuclear gas which is ionised and driven out along the radio jets (e.g. Begelman et al. 1984; Schulz 1988; Colbert et al. 1996, 1998) or photoionised ambient galactic gas (Pedlar et al. 1985; Unger et al. 1987; Falcke et al. 1998). This latter model²⁹ is consistent with the UV radiation ionising all of the gas, while giving a high UV luminosity in our direction. Furthermore, the paucity of extended ionised structures in type-1 Seyfert galaxies (Pogge 1989), which unified schemes dictate are intrinsically identical to their type-2 counterparts, suggests that these are being viewed at low inclinations and so do not extend beyond the central AGN from our viewpoint. Furthermore, *at all redshifts* (Fig. 9), all of the $\log L_{\text{UV}} \gtrsim 23$ radio sources have been flagged as quasars (by us as well as by

²⁸ <http://nedwww.ipac.caltech.edu/level5/Curran/frames.html>

²⁹ Where the torus may be a consequence of the weak radiation emitting from the equator of the continuum source, with the cone arising from gas ionised by the strong polar radiation (Pedlar et al. 1998).

Table 5. Partitioning of the 21-cm detections and non-detections with respect to $L_{UV} = 10^{23} \text{ W Hz}^{-1}$.

	$L_{UV} \lesssim 10^{23} \text{ W Hz}^{-1}$			$L_{UV} \gtrsim 10^{23} \text{ W Hz}^{-1}$		
	dets	nons	total	dets	nons	total
Galaxies	27	24	51	–	–	0
Quasars	6	12	18	0	16	16
Total	33	36	69	0	16	16

Vermeulen et al. 2003; Gupta et al. 2006)³⁰. That is, the sources in which the UV flux appears to be directed towards us are believed to be type-1 objects, in addition to having a very low (possibly zero) likelihood of exhibiting 21-cm absorption.

Although random orientation effects could give the 50% split of 21-cm detections and non-detections below the median value of $\log L_{UV} < 21.5$ (Sect. 3.1.2), at higher UV luminosities the number of 21-cm detections drops significantly, especially at $\log L_{UV} \gtrsim 23$. Also, for the low luminosity sample, there is a detection rate of 1/2 for the galaxies and 1/3 for the quasars (Table 5) and, while this is consistent with previous studies (Pihlström et al. 2003), the fact that the detection rate for the low UV luminosity quasars is significantly greater than for the $L_{UV} \gtrsim 10^{23} \text{ W Hz}^{-1}$ quasars (0/16), suggests that these may be different a beast than their low UV luminosity counterparts.

This is also illustrated in Fig. 9³¹, where it is seen that all of $z_{\text{em}} \gtrsim 1$ targets have UV luminosities in excess of $L_{UV} \sim 10^{22} \text{ W Hz}^{-1}$, demonstrating that there is a selection effect at play, where at high redshifts we are targetting the most optically bright sources, which are naturally better known at such high luminosity distances. At $z_{\text{em}} \lesssim 1$ (luminosity distances $\lesssim 6 \text{ Gpc}$), we see the whole range of luminosities. Again, the fact that all of the detections occur at $L_{UV} \lesssim 10^{23} \text{ W Hz}^{-1}$ is clearly evident, but whether the difference in luminosities is an intrinsic property is difficult to ascertain: The low UV luminosity quasars undetected in 21-cm absorption may be at sufficiently low inclinations so that a large column of neutral gas is not intercepted by the radio emission, while being inclined highly enough so that the axis of the jet does not cross our line of sight, i.e. the UV radiation is not directed towards us in these cases. Considering this, these low luminosity quasars may represent intermediate types (1 to 1.5, Keel 1980; Maiolino & Rieke 1995), which are known to have stronger ionisation lines than type-2 objects (Cohen 1983).

3.4.2 Orientation: Obscuration

If the orientation is important in the detection rate of H I absorption, one manifestation of it should be a higher extinction of the quasar emission by dust associated with the torus. We can test this via an optical–near-infrared colour–colour diagram, using the photometry in Appendix A, and in Fig. 10 we show the $V - R$ and $R - K$ colours, where available, for the sample. From this there is little apparent difference between the two populations: Although there are a few sources which lie off the main distribution in the direction expected from dust reddening, the bulk of the detections and non-detections are found to be concentrated in the same part of the plot. This indicates that the detections are not significantly more dust

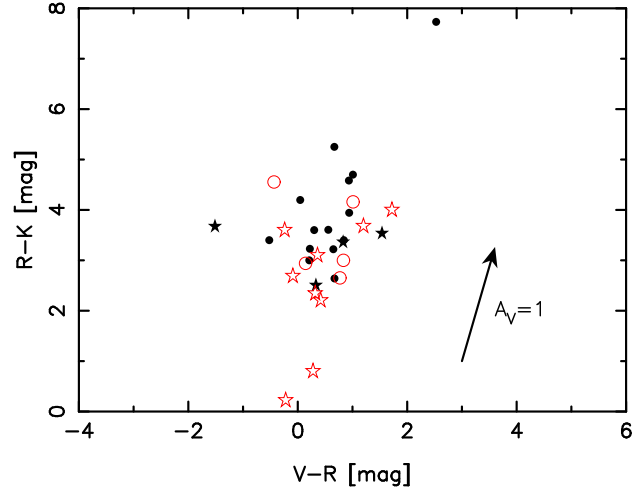


Figure 10. The $R - K$ colour versus the $V - R$ colour for the sample. As per Fig. 4, the filled symbols represent the 21-cm detections and the unfilled symbols the non-detections.

reddened than the non-detections. While this might indicate that the orientation hypothesis is not supported, it should be noted that if the dusty torus did significantly extinguish the quasar light, the host galaxy starlight would then dominate, lessening the apparent reddening.

As a check on the effect of orientation, we have examined the spectral type for each source in the full sample. This entailed an exhaustive literature search to find, ideally, published measurements of emission line fluxes, or alternatively, a published spectrum (Tables 6 and 7). This information was then used to classify the AGN as a type-1 (i.e. showing broad permitted lines), or a type-2, where only narrow lines are present. The result is shown in Fig. 9, where the detection rate for type-1 objects is 10/37, compared to 19/39 for the type-2s, indicating a preference for type-2 objects to exhibit 21-cm absorption.

If we split the sample at $L_{UV} = 10^{23} \text{ W Hz}^{-1}$, we see that all 16 of the high-luminosity sources are found to be type-1 objects. Being exclusive non-detections, this is in line with unified schemes. However, for the low luminosity sources, the detection rates are close to 50% for both types (10/21 for type-1s and 19/37 for type-2s). So while the raw detection rates for type-1s and type-2s appear different (actually only at a 1.95σ level), the dominant cause of the different detection rates between the type-1 and type-2 objects appears to be due to the 16 high-luminosity type-1 objects. Without these, i.e. for $L_{UV} < 10^{23} \text{ W Hz}^{-1}$, both AGN types have a $\sim 50\%$ probability of exhibiting H I absorption. In other words, a type-1 object does not automatically result in a non-detection of H I absorption, nor does a type-2 necessarily result in a detection. This flies in the face of the notion that the strength of the 21-cm absorption is determined by the aspect of the central obscuring torus (Sect. 3.2) and is strong evidence that the absorption occurs beyond the parsec-scale, possibly in the main disk of the galaxy, the orientation of which appears to have little bearing on the AGN type.

3.4.3 Host galaxy

The third point to consider is thus the quasar host galaxy. The detection of associated absorption simply requires that there is neutral gas at similar velocities to the quasar nucleus. While we have

³⁰ Although having classified all of the sources for ourselves (Sect. 3.2.2), not all of the assigned designations agree.

³¹ The symbols are discussed in the next section.

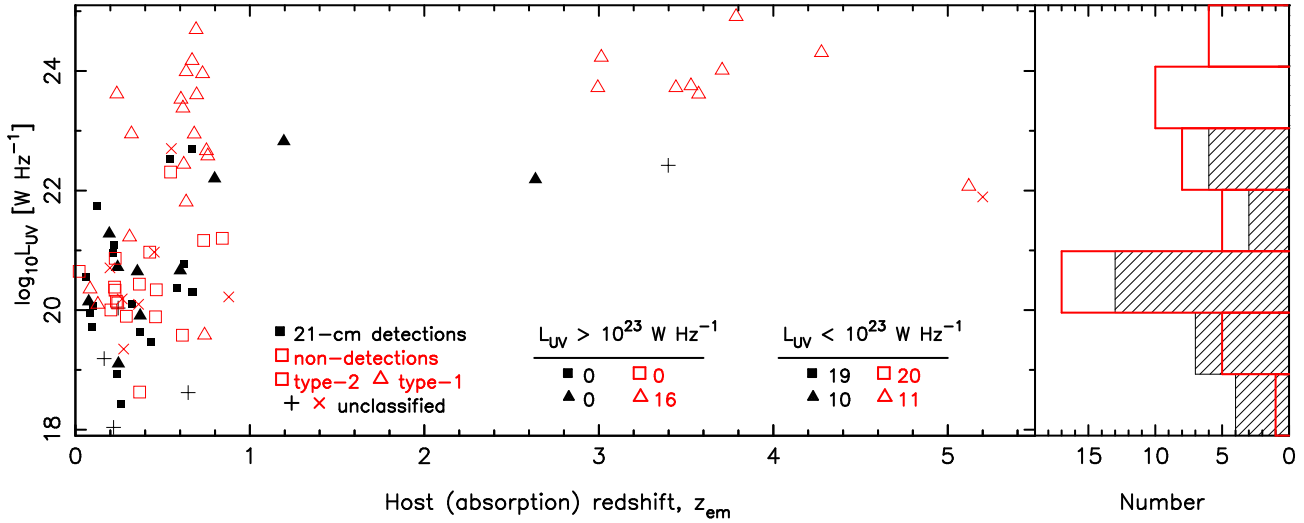


Figure 9. The ultra-violet luminosity–redshift distribution for the sample. The symbols and histograms are as per Fig. 4, but now the shapes represent the AGN classifications, with triangles representing type-1 objects and squares type-2s – the legend shows the number of each according to the UV luminosity cut-off (cf. Table 5). The distribution indicates that the extrapolations used for the low redshift sources (Sect. 3.1.2) do not appear to introduce an overwhelming bias in comparison to the high redshift sources (at least for the quasars). Should the extrapolations be overly erroneous, this would result in a systematic shift in the luminosities of the low redshift sample, although there would still be the sub-sample of those undetected in 21-cm absorption at higher UV luminosities.

been discussing the prospect of gas associated with the active nucleus (for instance, with the surrounding torus) and whether the nuclear obscuration plays a part, the rôle of gas in the host galaxy needs to be considered. Quasars, particularly at high redshifts, are observed to reside in galaxies of diverse types: For example, Peng et al. (2006) find that quasar hosts at $1 < z < 4.5$ span a range of morphologies consistent with early-types to disk/late-type galaxies. While some early-type galaxies are known from targeted searches to have significant H I content, particularly in the field (e.g. Morganti et al. 2006; Orienti et al. 2007), blind surveys, such as the ALFALFA survey (di Serego Alighieri et al. 2007), show that early type galaxies in clusters have a much lower neutral gas content. Those quasars with detected H I absorption are then more likely to be found in disk or late-type galaxies.

Our observed trend in the detection rate as a function of UV luminosity could thus be explained by a changing mix of host galaxy types, in the sense that a larger fraction of the more luminous quasars are found in early-type galaxies. While observational constraints limit our knowledge of such a tendency at $z > 2$, this trend is known to apply at lower redshifts. For instance, Taylor et al. (1996) find that the hosts of all radio-loud quasars studied, as well as the most powerful radio-quiet quasars (all with $z < 0.35$), have a de Vaucouleurs $r^{1/4}$ law profile (characteristic of elliptical galaxies), whereas the less powerful radio-quiet quasars exhibited exponential disc profiles. Taylor et al. (1996) suggest that the most luminous quasars reside in elliptical galaxies, regardless of their radio properties. More recent observations of $z < 0.3$ quasars, using adaptive optics (Guyon et al. 2006), find that most luminous quasars (with $L > 2L_H^*$) have elliptical host galaxies (this includes the majority of the radio-loud quasars). To summarise, in this scenario the most luminous quasars of our sample are in early-type galaxies, which have a lower neutral gas content than later types, and so the chance of detecting significant H I absorption is greatly reduced compared to the less-luminous quasars.

4 POSSIBLE EFFECTS IN THE NON-DETECTION OF MOLECULAR ABSORPTION

In light of the absence of atomic absorption due to the large UV luminosities, possibly due to unfavourable orientations, it is not surprising that molecular absorption remains undetected. However, were H I detected, a detectable molecular abundance would still not necessarily be expected from this sample, since:

(i) The relationship between molecular fraction and optical–near-infrared colour (Paper I) suggests that our sources would simply not be red enough to be detectable in molecular absorption at these sensitivities. The current sample had been selected before the conclusions of Paper I had been fully formulated, and so the range of $V - K$ colours most likely lie off to the left in Fig. 11 (the colours range from $V - K = 1.08 - 2.63$, where available).

(ii) Furthermore, due to the metallicity and molecular fraction evolution noted in DLAs (Curran et al. 2004b), at $z \geq 3$ we may expect much lower abundances than present day values. From a search of millimetre lines in DLAs with the Green Bank Telescope, Curran et al. (2004a) reached similar limits as this survey (Table 3). However, upon applying the molecular fraction evolution to the limits, they found that the survey was only sensitive of molecular fractions of close to unity, a value which even the DLAs detected in H₂ fall very far short of, although for $V - K \gtrsim 5.3$ such high fractions may be expected (figure 1 of Curran et al. 2006).

(iii) Lastly, at such high redshifts the cosmic microwave background will raise excitation temperatures of $T_x = 10$ K at $z = 0$ to $\gtrsim 20$ K. This has the effect of decreasing the sensitivities to these ground state transitions – by a factor of two for OH 18-cm ($^2\Pi_{3/2}J = 3/2$) and by up to a factor of four for the $J = 0 \rightarrow 1$ transitions (Curran et al. 2004a). One solution to this is to search higher transitions redshifted into the 3-mm band (cf. the 12-mm band), although lower flux densities, compounded with the need for much better observing conditions, makes this a poor trade.

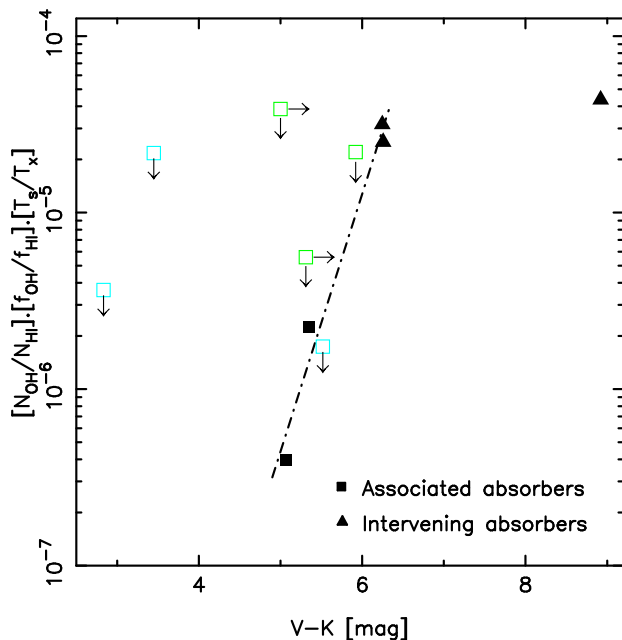


Figure 11. The normalised OH line strength ($2.38 \times 10^{14} \int \tau_{\text{OH}} dv / 1.82 \times 10^{18} \int \tau_{\text{HI}} dv$) versus optical-near-IR colour for the known OH absorbers. These are represented by the filled symbols, with the least-squares fit shown for the four millimetre systems. The correlation for the five OH absorbers is significant at the 2.0σ level, which rises to 3.0σ for the molecular fraction/ $V - K$ correlation for these sources plus the H_2 -bearing DLAs (figure 1 of Curran et al. 2006). The unfilled symbols show the other sources where H I has been detected and OH absorption searched: The three limits shown in figure 7 of Curran et al. (2006) [green] (the lower limits on the abscissa designate $R - K$ magnitudes) with a further three from Gupta et al. (2006) [blue]. Note that the OH limits have been rescaled according to the method described in Curran et al. (2007a), who find $\text{FWHM}_{\text{OH}} = \text{FWHM}_{\text{HI}}$ for the five known OH absorbers: Combining the otherwise unknown FWHM_{OH} with the optical depth limit, gives a more accurate estimate for the upper limit than quoting the column density limit per each Δv channel. This has the effect of degrading the apparent sensitivity, although some can be recovered since usually $\text{FWHM}_{\text{OH}} > \Delta v$. Therefore for the non-detections, we scale each of the OH column density limits by $\sqrt{\text{FWHM}_{\text{OH}}/\Delta v}$, thus giving the limit for a single channel “smoothed” to FWHM_{OH} . Associated absorption is designated by a square and intervening absorption (due to a gravitational lens) by a triangle.

5 SUMMARY

We have undertaken a survey for H I 21-cm and rotational molecular absorption in the hosts of radio sources at redshifts of $z \geq 2.9$, and report no detections in the 13 sources for which we have good data. Upon comparing our search criteria with those formulated in Paper I (Curran et al. 2006), we are not surprised that molecules (OH, HCN, HCO^+ & CO) were not detected in the 10 separate sources searched: With optical-near-infrared colours of $V - K \leq 2.63$ (at least where these are available), the sources do not exhibit the degree of reddening indicative of the dust abundances which would permit molecular fractions of close to unity, the limit to which current radio observations are sensitive.

However, since the co-moving density of H I at $z \sim 3$ is expected to be many times higher than present values (e.g. Péroux et al. 2001), the absence of detections of 21-cm absorption was surprising. We rule out the possibility that the non-detections are due exclusively to high 1420 MHz continuum fluxes maintaining an overpopulated 21-cm upper hyperfine (anti-parallel) level.

We do find, however, that all of our targets are quasars and the ultra-violet continuum luminosities are in excess of $L_{\text{UV}} \sim 10^{23} \text{ W Hz}^{-1}$. In comparison to the previous searches for redshifted 21-cm absorption:

- A mix of 21-cm detections and non-detections at lower redshifts (mostly $z \lesssim 1$) is well documented, where the detection rate is higher in galaxies than in quasars. This skew in the distribution is attributed to the possibility that radio galaxies are type-2 sources, whereas quasars are type-1 objects. That is, the more direct view to the active nucleus in a quasar means that the dusty obscuring torus, invoked by unified models, is orientated so that 21-cm absorption does not occur along our sight-line. Although our own low redshift results (Paper I) are consistent with this scenario, we find little evidence for a significantly higher degree of dust reddening by any obscuring gas in the 21-cm detections.

- Despite the fact that half of the whole $L_{\text{UV}} \gtrsim 10^{23} \text{ W Hz}^{-1}$ sample are at $z \leq 0.73$, this is the first time that a UV luminosity bias has been noted. The high UV luminosity again may be consistent with these being type-1 objects, where the bright UV continuum suggests we are seeing the accretion disk directly, unobscured by the circumnuclear torus. However, although random orientation effects can explain the mix of detections and non-detections in the low luminosity sample, the high luminosity sample, in which there are no detections, remains unexplained. This suggests that there are additional effects at play.

As well as several of our high redshift targets having intervening DLAs at similar redshifts to the background quasar, there exists a sample of proximate DLAs, where $z_{\text{abs}} \sim z_{\text{em}}$, and both of these groups show that large columns of neutral gas can in fact exist close to $L_{\text{UV}} \gtrsim 10^{23} \text{ W Hz}^{-1}$ QSOs. Since the gas in these intervening absorbers is not associated, and are thus free to have any aspect with respect to the AGN, this does not contradict the possibility that our non-detections are the result of orientation between the associated gas and the line-of-sight to the quasar. Furthermore, no other absorbers have been found closer to our targets (Ellison et al. 2001; Péroux et al. 2001), perhaps suggesting that either this gas is unfavourably orientated or that there is a proximity effect, where the intense UV radiation is photo-ionising the associated gas clouds (Bajtlik et al. 1988; Prochaska et al. 2008). This latter scenario could also be responsible for high spin temperatures in the DLAs towards our targets, which are sufficiently remote to host large columns of neutral gas, two of which have been searched and not detected in 21-cm absorption (Kanekar & Chengalur 2003).

Finally, although 21-cm absorption shows a slight preference to be present in galaxies over quasars, by determining the AGN spectroscopic type for each object (a total of 76), we find that below $L_{\text{UV}} \sim 10^{23} \text{ W Hz}^{-1}$ the presence of 21-cm absorption shows no preference for AGN type. That is, both type-1 and type-2 objects have a 50% likelihood of exhibiting 21-cm absorption and any apparent bias against type-1 objects is due solely to the 16 $L_{\text{UV}} \gtrsim 10^{23} \text{ W Hz}^{-1}$ objects. This means:

- (i) The ultra-violet luminosity, rather than the orientation of the AGN, can determine whether 21-cm absorption can be detected in the host galaxy, where at high luminosities 21-cm is never detected and at low luminosities the odds are even.

- (ii) The H I absorption probably does not occur in the obscuring torus, but in the large-scale galactic disk or is possibly associated with in-falling or out-flowing material (e.g. Jaffe & McNamara 1994; Pihlström et al. 1999; Morganti et al. 2001; Vermeulen et al.

2003). As such, there is as yet no definite explanation why there is only a 50% detection rate in $L_{UV} \lesssim 10^{23} \text{ W Hz}^{-1}$ sources.

(iii) If our classifications are to be trusted, although type-1 objects are more likely to arise in quasars and type-2s in galaxies, this is not the case for every object.

Whether all UV luminous sources arise in type-1 objects, is difficult to ascertain, and the fact that there are low UV luminosity non-detections is somewhat of a puzzle. If, as we believe, the absorption is occurring in the galactic disk, it may be the orientation of this which is responsible for the observed 21-cm optical depths. This would suggest that the galactic disk does not necessarily share a similar orientation to the dense circumnuclear gas on the parsec scale³². Alternatively, a possible explanation for the high luminosity non-detections is that this selection biases towards a specific class of host galaxy, i.e. gas-poor, early types, in our targets as well as the $L_{UV} \gtrsim 10^{23} \text{ W Hz}^{-1}$ quasars at $z \leq 0.73$. This may render the orientation argument also invalid in these cases.

The exclusive non-detections of 21-cm absorption for $L_{UV} \gtrsim 10^{23} \text{ W Hz}^{-1}$ quasars indicate why we do not see absorption in our PQFS sample. Our selection of targets was biased towards high UV luminosity sources in several ways. Firstly, the requirement of having a measured optical redshift preferentially selects objects that are relatively bright in the optical (i.e. rest-frame UV), where a suitable spectrum can be obtained in a feasible observing time. In the PQFS, 509 of the 878 sources have measured redshifts, so that about 42% of the sample is unavailable for this study. If anything, these missing sources would have luminosities lower than the quasars of our sample and so the detection of 21-cm absorption in any of these would have little bearing on our result.

Secondly, our high redshift selection clearly biases towards the brightest UV sources. This is despite our $B \gtrsim 19$ selection, which gives the luminosity ceiling of $L_{UV} \lesssim 3 \times 10^{24} \text{ W Hz}^{-1}$ at $z \sim 3$ ³³, well above the $10^{23} \text{ W Hz}^{-1}$ fiducial limit. Therefore, in order to detect associated H I at $z_{\text{em}} \geq 3$, sources with UV luminosities of $L_{UV} \lesssim 10^{23} \text{ W Hz}^{-1}$, should therefore be targeted. At luminosity distances of ≥ 24.5 Gpc, this corresponds to $\lambda \geq 4860 \text{ \AA}$ flux densities of $\lesssim 6 \mu\text{Jy}$, or $V \gtrsim 22$. For the one detection of associated H I at $z_{\text{em}} \geq 3$, $z_{\text{em}} = 3.3968$ in the radio galaxy 0902+343 (Uson et al. 1991), the observed flux density is $\approx 1 \mu\text{Jy}$, rendering this detectable towards a UV luminosity of $L_{UV} = 3 \times 10^{22} \text{ W Hz}^{-1}$, which is, not surprisingly, at the upper end of the 21-cm detections.

ACKNOWLEDGMENTS

We would like to thank the anonymous reviewer for their helpful and supportive comments. Christian Henkel for the 6-cm OH Einstein A-coefficients. Also, many thanks to Jim Lovell for performing all of the Tidbinbilla observations and the GMRT telescope operators for their extensive assistance.

We acknowledge financial support from the Access to Major

Research Facilities Programme which is a component of the International Science Linkages Programme established under the Australian Government's innovation statement, Backing Australia's Ability.

This research has made use of the NASA/IPAC Extragalactic Database (NED) which is operated by the Jet Propulsion Laboratory, California Institute of Technology, under contract with the National Aeronautics and Space Administration. This research has also made use of NASA's Astrophysics Data System Bibliographic Services.

This work made use of the Frequently Asked Questions of the Statistical Consulting Center for Astronomy, operated at the Department of Statistics, Penn State University, M.G. Akritas Director).

Funding for the Sloan Digital Sky Survey (SDSS) and SDSS-II has been provided by the Alfred P. Sloan Foundation, the Participating Institutions, the National Science Foundation, the U.S. Department of Energy, the National Aeronautics and Space Administration, the Japanese Monbukagakusho, and the Max Planck Society, and the Higher Education Funding Council for England. The SDSS Web site is <http://www.sdss.org/>.

REFERENCES

- Adelman-McCarthy J. K., et al., 2008, *ApJS*, 175, 297
- Allen D. A., Ward M. J., Hyland A. R., 1982, *MNRAS*, 199, 969
- Angonin-Willaime M.-C., Vanderriest C., Courbin F., Burud I., Magain P., Rigaut F., 1999, *A&A*, 347, 434
- Antonucci R. R. J., 1993, *ARA&A*, 31, 473
- Bahcall J. N., Ekers R. D., 1969, *ApJ*, 157, 1055
- Bajtlik S., Duncan R. C., Ostriker J. P., 1988, *ApJ*, 327, 570
- Begelman M. C., Blandford R. D., Rees M. J., 1984, *Reviews of Modern Physics*, 56, 255
- Carballo R., González-Serrano J. I., Benn C. R., Sánchez S. F., Vigotti M., 1999, *MNRAS*, 306, 137
- Carilli C. L., Menten K. M., Reid M. J., Rupen M. P., Yun M. S., 1998, *ApJ*, 494, 175
- Carilli C. L., Perlman E. S., Stocke J. T., 1992, *ApJ*, 400, L13
- Carilli C. L., Rupen M. P., Yanny B., 1993, *ApJ*, 412, L59
- Carilli C. L., Wang R., Hoven M., Dwarakanath K., Chengalur J., Wyithe S., 2007, *AJ*, 133, 2841
- Carrington A., Miller T. A., 1967, *Nat*, 214, 998
- Chandra S., Kegel W. H., Roy R. J. L., Hertenstein T., 1995, *A&AS*, 114, 175
- Chandra S., Maheshwari V. U., Sharma A. K., 1996, *A&AS*, 117, 557
- Chavushyan V., Mujica R., Gorshkov A. G., Konnikova V. K., Mingaliev M. G., Valdéz J. R., 2001, *Astronomy Reports*, 45, 79
- Chengalur J. N., de Bruyn A. G., Narasimha D., 1999, *A&A*, 343, L79
- Chu Y.-Q., Zhu X.-F., Butcher H., 1986, *Acta Astronomica Sinica*, 27, 151
- Chun M. R., Gharanfoli S., Kulkarni V. P., Takamiya M., 2006, *AJ*, 131, 686
- Cody A. M., Braun R., 2003, *A&A*, 400, 871
- Cohen R. D., 1983, *ApJ*, 273, 489
- Cohen R. D., Osterbrock D. E., 1981, *ApJ*, 243, 81
- Colbert E. J. M., Baum S. A., Gallimore J. F., O'Dea C. P., Christensen J. A., 1996, *ApJ*, 467, 551

³² Contradicting low redshift surveys (Keel 1980; Maiolino & Rieke 1995, and to a certain degree, Curran 2000a), which find that intermediate Seyferts of types 1, 1.2 and 1.5 will occur in face-on galaxies while those of type 1.8 and 1.9 will occur in the edge-on cases.

³³ The fact that one of our targets lies on the flux limit with $B = 19$, while also being the highest redshift source observed ($z = 3.8$), gives the one point above $L_{UV} = 3 \times 10^{24} \text{ W Hz}^{-1}$ (Fig. 9).

- Colbert E. J. M., Baum S. A., O'Dea C. P., Veilleux S., 1998, *ApJ*, 496, 786
- Combes F., Wiklind T., 1998, *ESO Messenger*, 91, 29
- Conway J., 1999, in Carilli C., Radford S., Menton K., Langston G., eds, *Highly Redshifted Radio Lines Vol. 156, HI Absorption from a Circumnuclear TORUS in the Hidden Quasar Cygnus A*, ASP Conf. Ser., p. 259
- Conway J. E., Blanco P. R., 1995, *ApJ*, 449, L131
- Curran S. J., 2000a, *A&AS*, 144, 271
- Curran S. J., 2000b, PhD thesis, Chalmers University of Technology
- Curran S. J., Darling J. K., Bolatto A. D., Whiting M. T., Bignell C., Webb J. K., 2007a, *MNRAS*, 382, L11
- Curran S. J., Johansson L. E. B., Rydbeck G., Booth R. S., 1998, *A&A*, 338, 863
- Curran S. J., Murphy M. T., Pihlström Y. M., Webb J. K., Bolatto A. D., Bower G. C., 2004a, *MNRAS*, 352, 563
- Curran S. J., Murphy M. T., Pihlström Y. M., Webb J. K., Purcell C. R., 2005, *MNRAS*, 356, 1509
- Curran S. J., Tzanavaris P., Murphy M. T., Webb J. K., Pihlström Y. M., 2007b, *MNRAS*, 381, L6
- Curran S. J., Tzanavaris P., Pihlström Y. M., Webb J. K., 2007c, *MNRAS*, 382, 1331
- Curran S. J., Webb J. K., 2006, *MNRAS*, 371, 356
- Curran S. J., Webb J. K., Murphy M. T., Bandiera R., Corbelli E., Flambaum V. V., 2002, *PASA*, 19, 455
- Curran S. J., Webb J. K., Murphy M. T., Carswell R. F., 2004b, *MNRAS*, 351, L24
- Curran S. J., Whiting M., Murphy M. T., Webb J. K., Longmore S. N., Pihlström Y. M., Athreya R., Blake C., 2006, *MNRAS*, 371, 431
- Dallacasa D., Falomo R., Stanghellini C., 2002, *A&A*, 382, 53
- Darling J., Giovanelli R., 2006, *AJ*, 132, 2596
- Darling J., Giovanelli R., Haynes M. P., Bower G. C., Bolatto A. D., 2004, *ApJ*, 613, L101
- de Koff S., Baum S. A., Sparks W. B., Biretta J., Golombek D., Macchetto F., McCarthy P., Miley G. K., 1996, *ApJS*, 107, 621
- de Vaucouleurs A., Longo G., 1988, *Catalogue of visual and infrared photometry of galaxies from 0.5 micrometer to 10 micrometer (1961-1985)*. University of Texas Monographs in Astronomy, Austin: University of Texas, 1988
- de Vries W. H., O'Dea C. P., Barthel P. D., Thompson D. J., 2000, *A&AS*, 143, 181
- de Vries W. H., O'Dea C. P., Baum S. A., Sparks W. B., Biretta J., de Koff S., Golombek D., Lehnert M. D., Macchetto F., McCarthy P., Miley G. K., 1997, *ApJS*, 110, 191
- de Vries W. H., O'Dea C. P., Perlman E., Baum S. A., Lehnert M. D., Stocke J., Rector T., Elston R., 1998, *ApJ*, 503, 138
- di Serego Alighieri S., et al., 2007, *A&A*, 474, 851
- Drinkwater M. J., et al., 1997, *MNRAS*, 284, 85
- Dunlop J. S., Peacock J. A., Savage A., Lilly S. J., Heasley J. N., Simon A. J. B., 1989, *MNRAS*, 238, 1171
- Eales S., Rawlings S., Puxley P., Rocca-Volmerange B., Kuntz K., 1993, *Nat*, 363, 140
- Eales S. A., 1985, *MNRAS*, 213, 899
- Eisenhardt P., Dickinson M., 1992, *ApJ*, 399, L47
- Ellison S. L., Hall P. B., Lira P., 2005, *AJ*, 130, 1345
- Ellison S. L., Yan L., Hook I. M., Pettini M., Wall J. V., Shaver P., 2001, *A&A*, 379, 393
- Ellison S. L., Yan L., Hook I. M., Pettini M., Wall J. V., Shaver P., 2002, *A&A*, 383, 91
- Eracleous M., Halpern J. P., 1994, *ApJS*, 90, 1
- Falcke H., Wilson A. S., Simpson C., 1998, *ApJ*, 502, 199
- Field G. B., 1959, *ApJ*, 129, 536
- Francis P. J., Whiting M. T., Webster R. L., 2000, *PASA*, 17, 56
- Fukugita M., Ichikawa T., Gunn J. E., Doi M., Shimasaku K., Schneider D. P., 1996, *AJ*, 111, 1748
- Gao Y., Solomon P. M., 2004, *ApJ*, 606, 271
- Gelderman R., Whittle M., 1994, *ApJS*, 91, 491
- Glikman E., Gregg M. D., Lacy M., Helfand D. J., Becker R. H., White R. L., 2004, *ApJ*, 607, 60
- Greenhill L. J., et al., 2003, *ApJ*, 590, 162
- Gregg M. D., Lacy M., White R. L., Glikman E., Helfand D., Becker R. H., Brotherton M. S., 2002, *ApJ*, 564, 133
- Gupta N., Saikia D. J., 2006a, *MNRAS*, 370, L80
- Gupta N., Saikia D. J., 2006b, *MNRAS*, 370, 738
- Gupta N., Salter C. J., Saikia D. J., Ghosh T., Jeyakumar S., 2006, *MNRAS*, 373, 972
- Gupta N., Srianand R., Petitjean P., Khare P., Saikia D. J., York D. G., 2007, *ApJ*, 654, L111
- Guyon O., Sanders D. B., Stockton A., 2006, *ApJS*, 166, 89
- Hambly N., et al., 2001, *MNRAS*, 326, 1279
- Heckman T. M., Lebofsky M. J., Rieke G. H., van Breugel W., 1983, *ApJ*, 272, 400
- Henkel C., Güsten R., Baan W. A., 1987, *A&A*, 185, 14
- Henstock D. R., Browne I. W. A., Wilkinson P. N., McMahon R. G., 1997, *MNRAS*, 290, 380
- Hewitt A., Burbidge G., 1989, *ApJS*, 69, 1
- Hirst P., Jackson N., Rawlings S., 2003, *MNRAS*, 346, 1009
- Hook I. M., Shaver P. A., Jackson C. A., Wall J. V., Kellermann K. I., 2003, *A&A*, 399, 469
- Hunstead R. W., Murdoch H. S., Shobbrook R. R., 1978, *MNRAS*, 185, 149
- Hyland A. R., Allen D. A., 1982, *MNRAS*, 199, 943
- Ishwara-Chandra C. H., Dwarakanath K. S., Anantharamaiah K. R., 2003, *JA&A*, 24, 37
- Jackson C. A., Wall J. V., Shaver P. A., Kellermann K. I., Hook I. M., Hawkins M. R. S., 2002, *A&A*, 386, 97
- Jackson N., Browne I. W. A., 1991, *MNRAS*, 250, 414
- Jaffe W., McNamara B. R., 1994, *ApJ*, 434, 110
- Kanekar N., Briggs F. H., 2003, *A&A*, 412, L29
- Kanekar N., Chengalur J. N., 2002, *A&A*, 381, L73
- Kanekar N., Chengalur J. N., 2003, *A&A*, 399, 857
- Kanekar N., Chengalur J. N., de Bruyn A. G., Narasimha D., 2003, *MNRAS*, 345, L7
- Kanekar N., Chengalur J. N., Lane W. M., 2007, *MNRAS*, 375, 1528
- Kanekar N., Subrahmanyam R., Ellison S. L., Lane W., Chengalur J. N., 2006, *MNRAS*, 370, L46
- Keel W. C., 1980, *AJ*, 85, 198
- Kim D.-C., Veilleux S., Sanders D. B., 1998, *ApJ*, 508, 627
- Kristian J., Sandage A., Katem B., 1974, *ApJ*, 191, 43
- Lanzetta K. M., Wolfe A. M., Turnshek D. A., Lu L., McMahon R. G., Hazard C., 1991, *ApJS*, 77, 1
- Lawrence C. R., Elston R., Januzzi B. T., Turner E. L., 1995, *AJ*, 110, 2570
- Lawrence C. R., Zucker J. R., Readhead A. C. S., Unwin S. C., Pearson T. J., Xu W., 1996, *ApJS*, 107, 541
- Lilly S., Longair M., 1984, *MNRAS*, 211, 833
- Lipovetsky V. A., Neizvestny S. I., Neizvestnaya O. M., 1988, *Soobshcheniya Spetsial'noj Astrofizicheskoy Observatorii*, 55, 5
- Lovell J. E. J., et al., 1996, *ApJ*, 472, L5
- Maiolino R., Rieke G. H., 1995, *ApJ*, 454, 95

- Marchã M. J., Caccianiga A., Browne I. W. A., Jackson N., 2001, *MNRAS*, 326, 1455
- Marchã M. J. M., Browne I. W. A., Impey C. D., Smith P. S., 1996, *MNRAS*, 281, 425
- Marziani P., Sulentic J. W., Dultzin-Hacyan D., Calvani M., Moles M., 1996, *ApJS*, 104, 37
- Marziani P., Sulentic J. W., Zamanov R., Calvani M., Dultzin-Hacyan D., Bachev R., Zwitter T., 2003, *ApJS*, 145, 199
- Mirabel I. F., 1989, *ApJ*, 340, L13
- Møller P., Warren S. J., Fynbo J. U., 1998, *A&A*, 330, 19
- Moore C. B., Carilli C. L., Menten K. M., 1999, *ApJ*, 510, L87
- Morganti R., et al., 2006, *MNRAS*, 371, 157
- Morganti R., Oosterloo T. A., Tadhunter C. N., van Moorsel G., Killeen N., Wills K. A., 2001, *MNRAS*, 323, 331
- O'Dea C. P., Baum S. A., Morris G. B., 1990, *A&AS*, 82, 261
- Orienti M., Morganti R., Dallacasa D., 2006, *A&A*, 457, 531
- Orienti M., et al., 2007, *New Astronomy Review*, 51, 8
- Overzier R. A., et al., 2006, *ApJ*, 637, 58
- Peck A. B., Taylor G. B., Conway J. E., 1999, *ApJ*, 521, 103
- Peck A. B., Taylor G. B., Fassnacht C. D., Readhead A. C. S., Vermeulen R. C., 2000, *ApJ*, 534, 104
- Pedlar A., Fernandez B., Hamilton N. G., Redman M. P., Dewdney P. E., 1998, *MNRAS*, 300, 1071
- Pedlar A., Unger S. W., Dyson J. E., 1985, *MNRAS*, 214, 463
- Peng C. Y., Impey C. D., Rix H.-W., Falco E. E., Keeton C. R., Kochanek C. S., Lehár J., McLeod B. A., 2006, *New Astronomy Review*, 50, 689
- Péroux C., Storrie-Lombardi L. J., McMahon R. G., Irwin M., Hook I. M., 2001, *AJ*, 121, 1799
- Pickett H. M., Poynter R. L., Cohen E. A., Delitsky M. L., Pearson J. C., Müller H. S. P., 1998, *J. Quant. Spectrosc. Radiat. Transfer*, 60, 883
- Pihlström Y. M., Conway J. E., Vermeulen R. C., 2003, *A&A*, 404, 871
- Pihlström Y. M., Vermeulen R. C., Taylor G. B., Conway J. E., 1999, *ApJ*, 525, L13
- Pihlström Y. M., Baan W. A., Darling J., Klöckner H.-R., 2005, *ApJ*, 618, 705
- Pogge R. W., 1989, *ApJ*, 345, 730
- Prestage R. M., Peacock J. A., 1983, *MNRAS*, 204, 355
- Prochaska J. X., Hennawi J. F., Herbert-Fort S., 2008, *ApJ*, 675, 1002
- Purcell E. M., Field G. B., 1956, *ApJ*, 124, 542
- Rao S., Turnshek D., Nestor D. B., 2006, *ApJ*, 636, 610
- Roche N., Eales S. A., 2000, *MNRAS*, 317, 120
- Rohlfs K., Wilson T. L., 2000, *Tools of Radio Astronomy*. Springer-Verlag, Berlin
- Sandage A., 1965, *ApJ*, 141, 1560
- Sandage A., 1973, *ApJ*, 183, 711
- Sandage A., Véron P., Wyndham J. D., 1965, *ApJ*, 142, 1307
- Schmitt H. R., Kinney A. L., 1996, *ApJ*, 463, 498
- Schneider D. P., et al., 2005, *AJ*, 130, 367
- Schulz H., 1988, *A&A*, 203, 233
- Simpson C., Rawlings S., 2000, *MNRAS*, 317, 1023
- Skrutskie M. F., et al., 2006, *AJ*, 131, 1163
- Smith E. P., Heckman T. M., 1989, *ApJS*, 69, 365
- Snellen I. A. G., Schilizzi R. T., Bremer M. N., Miley G. K., de Bruyn A. G., Röttgering H. J. A., 1999, *MNRAS*, 307, 149
- Spinrad H., Marr J., Aguilar L., Djorgovski S., 1985, *PASP*, 97, 932
- Srianand R., Khare P., 1993, *ApJ*, 413, 486
- Stanghellini C., O'Dea C. P., Baum S. A., Laurikainen E., 1993, *ApJS*, 88, 1
- Stickel M., Fried J. W., Kühr H., 1993, *A&AS*, 98, 393
- Stickel M., Kühr H., 1996, *A&AS*, 115, 11
- Stickel M., Kühr H., 1994, *A&AS*, 105, 67
- Stickel M., Rieke G. H., Kühr H., Rieke M. J., 1996, *ApJ*, 468, 556
- Stoeckle J. T., Wurtz R., Wang Q., Elston R., Jannuzi B. T., 1992, *ApJ*, 400, L17
- Stockton A., Ridgway S. E., 2001, *ApJ*, 554, 1012
- Subrahmanyan R., Narasimha D., Pramesh-Rao A., Swarup G., 1990, *MNRAS*, 246, 263
- Tadhunter C., Dickson R., Morganti R., Robinson T. G., Wills K., Villar-Martin M., Hughes M., 2002, *MNRAS*, 330, 977
- Tadhunter C. N., Morganti R., di Serego-Alighieri S., Fosbury R. A. E., Danziger I. J., 1993, *MNRAS*, 263, 999
- Taylor G. L., Dunlop J. S., Hughes D. H., Robson E. I., 1996, *MNRAS*, 283, 930
- Unger S. W., Pedlar A., Axon D. J., Whittle M., Meurs E. J. A., Ward M. J., 1987, *MNRAS*, 228, 671
- Urry C. M., Padovani P., 1995, *PASP*, 107, 803
- Uson J. M., Bagri D. S., Cornwell T. J., 1991, *PhRvL*, 67, 3328
- van Gorkom J. H., Knapp G. R., Ekers R. D., Ekers D. D., Laing R. A., Polk K. S., 1989, *AJ*, 97, 708
- Vermeulen R. C., et al., 2003, *A&A*, 404, 861
- Vermeulen R. C., Taylor G. B., 1995, *AJ*, 109, 1983
- Vermeulen R. C., Taylor G. B., Readhead A. C. S., Browne I. W. A., 1996, *AJ*, 111, 1013
- Weymann R. J., Carswell R. F., Smith M. G., 1981, *ARA&A*, 19, 41
- White R. L., et al., 2000, *ApJS*, 126, 133
- Wiklind T., Combes F., 1994, *A&A*, 286, L9
- Wiklind T., Combes F., 1995, *A&A*, 299, 382
- Wiklind T., Combes F., 1996a, *Nat*, 379, 139
- Wiklind T., Combes F., 1996b, *A&A*, 315, 86
- Wiklind T., Combes F., 1998, *ApJ*, 500, 129
- Wilkes B. J., Wright A. E., Jauncey D. L., Peterson B. A., 1983, *PASA*, 5, 2
- Wills D., Lynds R., 1978, *ApJS*, 36, 317
- Winn J. N., Morgan N. D., Hewitt J. N., Kochanek C. S., Lovell J. E. J., Patnaik A. R., Pindor B., Schechter P. L., Schommer R. A., 2002, *AJ*, 123, 10
- Wolfe A. M., Burbidge G. R., 1975, *ApJ*, 200, 548
- York B. A., Kanekar N., Ellison S. L., Pettini M., 2007, *MNRAS*, 382, L53
- York D. G., Adelman J., Anderson Jr. J. E., Anderson S. F., Annis J., Bahcall N. A., Bakken J. A., Barkhouser R., Bastian 2000, *AJ*, 120, 1579
- Zheng Z., Miralda-Escudé J., 2002, *ApJ*, 568, L71
- Zickgraf F.-J., Voges W., Krautter J., Thiering I., Appenzeller I., Mujica R., Serrano A., 1997, *A&A*, 323, L21

APPENDIX A

In this section we list all of the sources used in the analysis, which all been obtained from the literature cited in Table 1, complete with the compiled photometry and classification.

Table 6. The sources detected in 21-cm absorption, listed by their B1950.0 or J2000.0 name as given in the 21-cm search paper (Table 1). The final columns give the estimated luminosity at 1216Å [W Hz⁻¹] and our determination of the AGN type.

Source	Class	z_{em}	B [mag]	Ref	V [mag]	Ref	R [mag]	Ref	K [mag]	Ref	$\log L_{\text{UV}}$ [W Hz ⁻¹]	Type	Ref
J0025-2602	Gal	0.3220	20.300	30	—	—	18.084	30	15.674	61	20.100	2	75
0108+388	Gal	0.6685	—	—	—	—	22.000	65	16.690	71	20.309	2	43
J0119+3210	Gal	0.0600	16.271	30	—	—	14.749	30	12.600	31	20.548	2	28
J0141+1353	Gal	0.6210	22.327	30	20.920	27	20.876	30	16.680	27	20.777	2	64
J0414+0534	Gal	2.6365	24.100	29	23.800	42	21.270	3	13.540	42	22.188	1	42
J0410+7656	Gal	0.5985	—	—	—	—	21.200	70	—	—	—	2	43
J0431+2037	Gal	0.2190	22.174	30	—	—	19.085	30	14.924	16	18.039	—	—
0500+019	Gal	0.5846	22.500	17	21.350	8	20.682	8	15.430	24	20.367	2	35
0758+143	QSO	1.1946	19.976	30	17.460	57	18.972	30	15.300	60	22.825	1	73
J0834+5534	Gal	0.2420	18.921	30	17.390	1	17.180	46	14.180	61	20.719	1	1
J0901+2901	Gal	0.1940	19.321	30	18.078	1	18.600	12	15.200	16	21.280	1	26
0902+343	Gal	3.3980	—	—	23.800	8	23.500	21	19.900	21	22.422	—	20
J0909+4253	QSO	0.6700	18.960	4	19.049	1	18.220	4	14.860	60	22.699	2	1
J1124+1919	Gal	0.1650	22.082	30	21.448	1	20.513	30	15.930	16	19.190	—	—
J2032+1707	Gal	0.2170	18.758	30	—	—	17.327	30	14.864	61	20.949	2	11
J1206+6413	Gal	0.3710	21.847	30	20.790	1	19.910	55	—	—	19.908	1	26
J1326+3154	Gal	0.3700	21.367	30	19.822	1	18.882	30	14.940	16	19.638	2	18
J1347+1217	QSO	0.1217	16.615	62	16.050	62	15.718	30	13.216	61	21.736	2	39
J1357+4354	Gal	0.6460	—	—	22.708	1	20.951	30	—	—	18.620	—	—
J1400+6210	Gal	0.4310	22.137	30	20.373	1	19.530	30	16.130	16	19.459	2	43
J1407+2827	Gal	0.0766	16.345	30	14.910	13	14.240	13	11.601	61	20.144	1	23
1413+135	QSO	0.2467	21.055	30	20.000	33	18.461	30	14.928	61	19.105	1	72
1504+377	Gal	0.6715	—	—	21.808	1	20.800	69	16.100	71	20.295	2	69
1555-140	Gal	0.0970	18.280	25	16.930	25	16.280	25	13.060	25	19.719	2	79
J1815+6127	QSO	0.6010	21.272	30	—	—	19.122	30	—	—	20.665	1	76
J1816+3457	Gal	0.2448	20.342	30	—	—	18.459	30	15.525	61	20.034	—	—
J1821+3942	Gal	0.7980	19.598	30	—	—	18.135	30	15.023	61	22.202	1	77
J1944+5448	Gal	0.2630	21.732	30	—	—	18.591	30	15.000	61	18.424	2	67
J1945+7055	Gal	0.1010	18.726	30	—	—	17.199	30	13.369	61	20.067	2	67
J2052+3635	Gal	0.3550	22.083	30	—	—	21.200	30	—	—	20.648	1	14
J2245+3941	Gal	0.0811	17.788	30	16.550	58	15.993	30	12.388	61	19.947	2	43
J2255+1313	QSO	0.5430	19.535	30	19.590	1	19.190	15	—	—	22.530	2	26
J2316+0405	Gal	0.2199	18.595	62	17.440	62	17.220	30	13.991	61	21.081	2	74
J2355+4950	Gal	0.2379	21.101	30	—	—	18.400	51	15.112	61	18.940	2	43

References: (1) SDSS DR6, Adelman-McCarthy et al. (2008), (2) Allen et al. (1982), (3) Angonin-Willaime et al. (1999), (4) Carballo et al. (1999), (5) Chavushyan et al. (2001), (6) Chu et al. (1986), (7) Chun et al. (2006), (8) Cody & Braun (2003), (9) Cohen & Osterbrock (1981), (10) Dallacasa et al. (2002), (11) Darling & Giovanelli (2006), (12) de Koff et al. (1996), (13) de Vaucouleurs & Longo (1988), (14) de Vries et al. (2000), (15) de Vries et al. (1997), (16) de Vries et al. (1998), (17) Drinkwater et al. (1997), (18) Dunlop et al. (1989), (19) Eales (1985), (20) Eales et al. (1993), (21) Eisenhardt & Dickinson (1992), (22) Ellison et al. (2005), (23) Eracleous & Halpern (1994), (24) P. Francis (priv. comm.), (25) Francis et al. (2000), (26) Gelderman & Whittle (1994), (27) Glikman et al. (2004), (28) Gao & Solomon (2004), (29) Gregg et al. (2002), (30) SuperCOSMOS Sky Survey, Hambly et al. (2001), (31) Heckman et al. (1983), (32) Henstock et al. (1997), (33) Hewitt & Burbidge (1989), (34) Hirst et al. (2003), (35) Hook et al. (2003), (36) Hunstead et al. (1978), (37) Hyland & Allen (1982), (38) Jackson & Browne (1991), (39) Kim et al. (1998), (40) Kristian et al. (1974), (41) Lanzetta et al. (1991), (42) Lawrence et al. (1995), (43) Lawrence et al. (1996), (44) Lilly & Longair (1984), (45) Lipovetsky et al. (1988), (46) Marchã et al. (2001), (47) Marchã et al. (1996), (48) Marziani et al. (2003), (49) Marziani et al. (1996), (50) NASA Extragalactic Database (NED), (51) O’Dea et al. (1990), (52) Overzier et al. (2006), (53) Prestage & Peacock (1983), (54) Rao et al. (2006), (55) Roche & Eales (2000), (56) Sandage et al. (1965), (57) Sandage (1965), (58) Sandage (1973), (59) Schneider et al. (2005), (60) Simpson & Rawlings (2000), (61) 2MASS, Skrutskie et al. (2006), (62) Smith & Heckman (1989), (63) Snellen et al. (1999), (64) Spinrad et al. (1985), (65) Stanghellini et al. (1993), (66) Stickel et al. (1993), (67) Srianand & Khare (1993), (68) Stickel & Kühr (1996), (69) Stickel & Kühr (1994), (70) Schmitt & Kinney (1996), (71) Stickel et al. (1996), (72) Stocke et al. (1992), (73) Stockton & Ridgway (2001), (74) Tadhunter et al. (2002), (75) Tadhunter et al. (1993), (76) Vermeulen & Taylor (1995), (77) Vermeulen et al. (1996), (78) White et al. (2000), (79) Wilkes et al. (1983), (80) Wills & Lynds (1978), (81) Winn et al. (2002), (82) Zickgraf et al. (1997),

APPENDIX B

The ultraviolet luminosities (Sect. 3.1.2) are calculated at a standard rest-frame wavelength for each source, in this case $\lambda_U = 1216$ Å. As before (Sect. 3.1.1), the luminosity is given by the expression $L_{\lambda_U} = 4\pi D_{\text{QSO}}^2 F_{\lambda_U(1+z)}/(z_{\text{em}} + 1)$, although rather than using a K -correction term, to correct a given observed

passband to the appropriate rest-frame wavelength, we instead interpolate between or extrapolate from the observed photometry to obtain the flux at the observed wavelength $\lambda_U(z + 1)$.

The extrapolation or interpolation is done by fitting a power law (i.e. a linear fit in $\log \lambda - \log F$ space). Thus, for two observations at bands 1 and 2, with fluxes F_1 and F_2 , the UV flux is

Table 7. As Table 6 but for the sources not detected in 21-cm absorption.

Source	Class	z_{em}	B [mag]	Ref	V [mag]	Ref	R [mag]	Ref	K [mag]	Ref	$\log L_{\text{UV}}$ [W Hz $^{-1}$]	Type	Ref
J0003+2129	QSO	0.4520	21.005	30	20.580	10	19.650	10	—	—	20.971	—	—
0131-001	QSO	0.8790	23.340	25	22.500	25	20.780	25	16.780	25	20.221	—	—
J0157-1043	QSO	0.6160	17.504	30	—	—	17.039	30	—	—	23.380	1	48
J0201-1132	QSO	0.6690	16.232	30	—	—	16.073	30	13.860	37	24.176	1	75
J0224+2750	Gal	0.3102	19.502	30	—	—	18.263	30	15.250	44	21.225	1	23
0335-122	QSO	3.4420	21.018	30	20.110	22	20.199	30	17.510	22	23.722	1	6
0347-211	QSO	2.9940	20.476	30	—	—	20.297	30	17.900	—	23.722	1	35
J0348+3353	Gal	0.2430	20.723	30	—	—	19.110	15	14.390	16	20.121	2	23
J0401+0036	Gal	0.4260	20.200	40	19.010	40	18.532	30	—	—	20.969	2	9
J0521+1638	QSO	0.7590	19.370	56	18.840	56	18.480	15	15.380	60	22.580	1	26,38
0537-286	QSO	3.0140	19.290	17	—	—	18.789	30	16.770	24	24.231	1	79
J0542+4951	QSO	0.5450	18.450	57	17.800	57	17.210	15	—	—	22.311	2	26,34
J0556-0241	Gal	0.2350	20.968	30	—	—	19.533	30	—	—	20.150	2	14
J0609+4804	Gal	0.2769	21.198	30	—	—	18.767	30	—	—	19.349	—	—
J0655+4100	Gal	0.0216	15.021	30	—	—	13.996	30	10.357	61	20.648	2	47
J0709+7449	Gal	0.2921	19.982	30	—	—	17.540	19	13.790	53	19.898	2	50
J0741+3112	QSO	0.6350	16.517	30	16.100	54	16.322	30	16.100	7	23.990	1	1
J0815-0308	Gal	0.1980	18.490	62	16.940	62	16.797	30	13.858	61	20.707	—	—
J0840+1312	QSO	0.6808	18.370	80	17.940	80	17.622	30	15.280	60	22.947	1	49
J0913+5919	QSO	5.1200	—	—	23.281	1	24.948	1	—	—	22.071	1	1
J0924-2201	Gal	5.2000	—	—	—	—	25.850	52	—	—	21.893	—	—
J0927+3902	QSO	0.6948	17.064	30	—	—	16.486	30	—	—	23.603	1	1
J0939+8315	Gal	0.6850	—	—	—	—	20.140	44	—	—	—	2	64
J0943-0819	Gal	0.2280	19.401	30	—	—	18.100	70	14.750	16	20.868	2	14
J0954+7435	Gal	0.6950	—	—	—	—	21.700	70	—	—	—	—	—
1026+084	QSO	4.2760	21.070	30	—	—	19.154	30	—	—	24.308	1	82
J1035+5628	Gal	0.4590	—	—	21.244	1	20.200	65	—	—	19.889	2	43
J1120+1420	Gal	0.3620	—	—	20.935	1	20.100	30	17.100	16	20.098	—	—
J1159+2914	QSO	0.7290	17.489	30	18.113	1	17.652	30	—	—	23.955	1	78
1228-113	QSO	3.5280	22.010	17	—	—	19.115	30	16.370	24	23.754	1	17
J1252+5634	QSO	0.3210	17.760	56	17.930	56	17.660	15	—	—	22.949	1	1
J1308-0950	Gal	0.4640	20.767	30	20.500	53	18.439	30	—	—	20.340	2	75
J1313+5458	QSO	0.6130	—	—	21.735	1	20.374	30	—	—	19.581	2	77
1351-018	QSO	3.7070	21.030	17	19.696	1	19.277	30	17.070	24	24.014	1	59
J1421+4144	Gal	0.3670	20.496	30	19.330	1	18.560	19	15.910	44	20.435	2	50
J1443+7707	Gal	0.2670	—	—	—	—	18.730	15	—	—	—	2	26
1450-338	Gal	0.3680	22.520	25	20.400	25	19.390	25	15.230	25	18.629	2	17
J1511+0518	Gal	0.0840	17.993	30	16.200	40	16.634	30	12.081	61	20.353	1	5
1535+004	QSO	3.4970	—	—	—	—	—	—	19.540	24	—	—	—
J1540+1447	QSO	0.6050	17.480	80	17.000	80	17.240	30	13.640	2	23.529	1	66
J1546+0026	Gal	0.5500	19.730	80	18.900	80	—	—	16.420	16	22.703	—	—
J1623+6624	Gal	0.2030	19.477	30	—	—	17.430	30	—	—	20.004	2	63
J1642+6856	QSO	0.7510	19.723	30	—	—	19.219	30	—	—	22.667	1	43
J1658+0741	QSO	0.6210	19.993	30	—	—	19.598	30	—	—	22.441	1	79
J1823+7938	Gal	0.2240	19.269	30	—	—	17.415	30	13.866	61	20.385	2	32
J1829+4844	QSO	0.6920	16.260	30	—	—	16.860	15	14.250	60	24.692	1	26
J1831+2907	Gal	0.8420	21.917	30	—	—	20.200	30	—	—	21.201	2	68
J1845+3541	Gal	0.7640	—	—	—	—	21.900	65	—	—	—	2	77
1937-101	QSO	3.7870	18.800	30	—	—	17.188	30	13.816	61	24.910	1	41
J2022+6136	Gal	0.2270	19.830	30	—	—	18.146	30	—	—	20.334	2	26
J2137-2042	Gal	0.6350	20.400	53	—	—	19.286	30	—	—	21.808	1	74
2149+056	QSO	0.7400	23.700	25	22.050	25	20.850	25	17.170	25	19.582	1	68
2215+02	QSO	3.5720	21.840	25	20.420	25	20.140	25	19.340	25	23.613	1	17
J2250+1419	QSO	0.2370	16.760	80	16.640	80	17.243	30	—	—	23.616	1	1
2300-189	Gal	0.1290	18.430	17	—	—	16.569	30	13.060	61	20.099	1	36
J2321+2346	Gal	0.2680	20.315	30	—	—	18.468	30	14.710	16	20.187	—	—
J2344+8226	QSO	0.7350	21.769	30	—	—	20.220	70	15.850	16	21.165	2	43

$$F_{\lambda_U(1+z)} = F_1 \left(\frac{\lambda_U(1+z)}{\lambda_1} \right)^\alpha, \text{ where } \alpha = \frac{\log(F_2/F_1)}{\log(\lambda_2/\lambda_1)}.$$

Although the observational data we have obtained from the literature is a heterogeneous mix of photometry, we try as much as possible to maintain consistency by using the same bands. The combination that covers the largest number of sources is *B* and *R* bands. Due to the relatively low redshift of most of the sources, extrapolation from *B* band is required. If *B* is not available, *V* is used instead, and if one of *V* or *R* is not available, *K* band was used. In one case, J0924–2201, only *R* was used since the high redshift meant that $\lambda_U(1+z)$ fell into this band.